Imbalance in the modern hydrologic budget of topographic catchments along the western slope of the Andes (21–25°S)

David F. Boutt[1], Lilly G. Corenthal[1], LeeAnn Munk[2], Scott A. Hynek[3],

[1] Department of Geosciences, University of Massachusetts-Amherst, Amherst, MA, USA

[2] Department of Geological Sciences, University of Alaska-Anchorage, Anchorage, AK, USA

[3] Earth and Environmental Systems Institute and Department of Geosciences, Pennsylvania State University, University Park, PA, USA

Mailing Address:

Department of Geosciences
611 North Pleasant Street
233 Morrill Science Center
University of Massachusetts
Amherst, MA 01003-9297

Key Points

- Modern hydrologic budgets in topographic watersheds along the western margin of the Andes (21–25°S) do not close.
- Steady state regional flow from outside these basins yield large contributing areas of conflicting nature.
- Transient groundwater storage is essential to balance water budget and is consistent with paleohydrologic observations.

Keywords: Salar de Atacama, Chile, recharge, regional groundwater flow, plateau, paleo-recharge, pulsed recharge, recharge events

Abstract

Rates of water discharge often exceed groundwater recharge in arid catchments. This apparent mass imbalance within a catchment may be reconciled through either regional-scale groundwater flow between topographic drainages and/or the draining of stored groundwater recharged during pluvial periods. We investigate discrepancies in the modern hydrologic budget of catchments along the west flank of the Andes in northern Chile (21–25° S), focused on the endorheic Salar de Atacama basin, and adjacent basins. Our new, uncertainty bounded, estimates of modern recharge rates do not come close to balancing observed modern groundwater discharge within topographic catchments. Two geologically realistic conceptualizations of hydrogeologic catchments discharging to Salar de Atacama were explored with a 2D groundwater model. Results from models support the interpretation that both regional flow and transient drainage of groundwater from storage are required to balance water budgets along the plateau margin. The models further examine whether this system is still responding to climatic forcing from pluvial periods and highlight general characteristics for similar plateau margin systems including: (1) water level changes at the plateau margin are highly sensitive to changes in recharge on the plateau, (2) extent and magnitude of the changes in water table are controlled by the distribution of hydraulic conductivity at the margin, (3) contributing area to the lower elevation catchment is itself dynamic, and not coincident with the topographic boundary, and (4)

difficulty in reconciling the modern position of "the water table" on the Andean plateau with the regional groundwater flow conceptualization and modern discharge to low lying catchments.

1. Introduction

Rates of anthropogenic water extraction and natural water discharge often exceed groundwater recharge in arid catchments [e.g. *van Beek et al.*, 2011; *Gleeson et al.*, 2012]. This mass imbalance within a catchment may be reconciled by regional-scale groundwater flow between topographic drainages and/or the draining of stored groundwater recharged during past pluvial periods. While these processes are well documented globally [e.g. *Alley et al.*, 2002; *Gleeson et al.*, 2011; *Condon and Maxwell*, 2015], debates exist over methods to physically and quantitatively distinguish between these mechanisms since both depend on processes operating on large spatial and temporal scales difficult to directly observe [e.g. *Nelson et al.*, 2004; *Masbruch et al.*, 2016; *Nelson and Mayo*, 2014]. Both mechanisms invalidate the steady state assumption often targeted for water resource management [e.g. Salar de Atacama (SdA) in *Dirección General de Aguas*, 2013; *Gorelick and Zheng*, 2015; *Currell et al.*, 2016]; this assumption also underpins lake-based paleo-precipitation reconstructions [e.g. *Urbano et al.*, 2004]. Therefore, we aim to better constrain the spatial and temporal dimensions of regional-scale groundwater flow and transient draining of groundwater storage at a site where extreme modern hydrologic imbalance is documented in the topographic watershed.

Plateau margins, especially in arid regions, are characterized by steep gradients in topography and climate that are conducive to the development of regional-scale groundwater systems [*Haitjema and Mitchell-Bruker*, 2005; *Gleeson et al.*, 2011]. Closed basins within or adjacent to plateau may preserve geologic records of water fluxes over 10^2–10^6 year time frames in the accumulation of evaporite minerals [e.g. *Godfrey et al.*, 2003; *Jordan et al.*, 2007; Munk et al., 2018]. The Salar de Atacama (SdA) hosts >1800 km^3 of halite in a closed basin adjacent to the Altiplano-Puna plateau, and provides an extreme case to evaluate the potential role of regional-scale groundwater flow and transient draining of groundwater storage in sustaining water discharge rates over both modern and geologic timescales (Figure 1).

Sustaining the accumulation of massive (>1500 m thick [*Jordan et al.*, 2007]) evaporites in the basin necessitates maintaining the water table within several meters of land surface over a 5–10 million year time period [*Tyler et al.*, 2006]. Individual components of the water budget of the relatively small and hyperarid topographic watershed of SdA, and of the adjacent Altiplano-Puna plateau [*Kampf and Tyler*, 2006; *Salas et al.*, 2010] have been studied extensively. While evidence for modern recharge in the central Andes exists [*Houston*, 2007, 2009]; rates, spatial extent, and mechanisms are poorly constrained [e.g. *Montgomery et al.*, 2003; *Jordan et al.*, 2015; *Rissmann et al.*, 2015]. Halite accumulation, a proxy for long term average water inflow, confirms the observed hydrologic imbalance over geologically meaningful timescales [up to 10 Myr; *Corenthal et al.*, 2016]. However, recently Munk et al. (2018) presented solute fluxes for the surface and shallow sub-surface that account for halite and brine hosted solutes in the uppermost (30 m) on a Myr timescale. Regional scale groundwater flow, interbasin transfer, and pulsed recharge events (10–100 year timescale) are documented [*Houston*, 2006b; *Rissmann et al.*, 2015] in the region, and. modern discharge in the Atacama Desert is suggested to reflect the draining of groundwater recharged during episodic pluvial periods (10^3–10^4 year timescale) in the Late Pleistocene and Holocene [*Houston and Hart*, 2004; *Gayo et al.*, 2012].

Previous efforts to balance the water budget of SdA [*Dirección General de Aguas*, 2013; *Rissmann et al.*, 2015; *Corenthal et al.,* 2016], nearby closed basins [*Houston and Hart*, 2004], and plateau margins in general [e.g. *Andermann et al.*, 2012] identified large uncertainties in water flux estimates. Here, recharge from precipitation is quantified by scaling point measurements to regional satellite datasets including uncertainty, further defining the magnitude and time-scale of the hydrologic imbalance inferred from observations of halite accumulation in SdA [*Corenthal et al.,* 2016]. Unique datasets are integrated to: (1) quantify the area of a regional-scale groundwater catchment necessary to balance modern discharge, and (2) approximate the role of late-Pleistocene recharge in modern discharge, and (3) elucidate the mechanisms and process by which water is delivered to the basin. These data are then used to constrain a 2D groundwater model that further explores the dynamic temporal and spatial scales of both regional groundwater flow and transient drainage in two hydrogeologicalconceptualizations. The focused nature of groundwater discharge allows reassessment of the contributing areas of plateau margins, and steady state water management strategies that may apply to similar arid, high-relief regions globally.

1.1 Regional Geologic and Hydrologic Framework

Salar de Atacama (SdA), a significant topographic depression with an area over 17,000 km^2 adjacent to the Altiplano-Puna plateau of the Central Andes, serves as the focal point for our analysis of the hydrologic imbalance in the region (Figure 1). SdA began accumulating a massive halite deposit ~7 Ma, coincident with uplift of the Central Andean Plateau [*Jordan et al.*, 2002a, 2007; *Reutter et al.*, 2006]. The halite nucleus of the basin hosts a lithium-rich brine that provides approximately one-third of the global lithium supply [*Maxwell*, 2014]. Alluvial fans conduct water to SdA, and numerous springs and seeps discharge in the transition zone around the halite nucleus, supporting environmentally sensitive wetlands and lagoons. The spatial trend of alluvium, carbonate, gypsum and halite downgradient along flowpaths through the transition zone documents the evaporation of inflow water until it reaches halite saturation [*Risacher et al.*, 2003]. Seven perennial and ephemeral streams emerge at stratigraphic and structural contacts but lose all surface flow through alluvium before reaching gypsum and halite facies, however, shallow groundwater again emerges in complex lagoon systems above a freshwater/brine interface that rims the salar margin. A series of hydrogeologically important Plio-Pleistocene ignimbrites originate from the Altiplano-Puna Volcanic Complex on the plateau [e.g. *Jordan et al.*, 2007; *Salisbury et al.*, 2011] and extend into the SdA subsurface; in the northern half of the basin these units are interpreted to be highly continuous. The north-south trending blind, high-angle, down-to-the-east Salar Fault System accommodates over 1 km of offset through the halite nucleus [*Lowenstein et al.*, 2003; *Jordan et al.*, 2007; Rubilar et al., 2017; Martinez et al., 2018]. *Jordan et al.* [2002] suggest that this fault acts as a barrier causing orogenic scale groundwater flow paths to discharge in SdA.

There are many studies that either explicitly document [*Magaritz et al.*, 1990; *Montgomery et al.*, 2003; *Rissmann et al.*, 2015; *Jayne et al.,* 2016] or implicate [*Pérez-Fodich et al.*, 2014; *Jordan et al.*, 2002a, 2002b] that water from the Andean Cordillera via regional groundwater flow feeds downgradient basins to the west. In their analysis on the MNT aquifer, Rissman et al. [2015] provide one of the few examples in the region where hydrologic and geochemical information have been used to investigate and imply a connection from a high elevation recharge area southeast of SdA to discharge at the salar margin. The $^{87}Sr/^{86}Sr$ values for discharging water reported by Munk et al. [2018] support the possible link between high elevation salt lakes and brines in SdA proposed by Rissman et al. [2015], and consistent with the observation of Grosjean et al. [1995] that many of the high elevation lakes never reach Na-Cl saturation and that the water enriched in Na and Cl then drains to lower elevation basins. Investigation and refinement of the hydrogeologic framework for many such aquifers is required to understand the regional scale imbalances in water budgets, and we embark on broad scale characterization of such systems in this work.

The SdA basin, in the core of Atacama Desert, is characterized by a hyperarid to arid climate [*Hartley and Chong*, 2002]. Significant inter-annual precipitation variability [*Garreaud et al.*, 2003] includes infrequent high-intensity rainfall events that produce pulsed groundwater recharge [*Houston*, 2006b; *Boutt et al., 2016*]. Because the basin has been closed since at least the late Miocene [*Jordan et al.*, 2002a], surface water discharge occurs only through evapotranspiration. Sedimentary records suggest that variable arid to hyperarid climates have dominated since 53 ka [*Bobst et al.*, 2001; *Godfrey et al.*, 2003], with at least four periods wetter than modern occurring since 106 ka [*Gayo et al.*, 2012]. Hydrologic models for lakes in the Bolivian Altiplano similarly suggest that precipitation may have been 2–3 times more than the modern during at least four intervals in the previous 130 ka, with the most recent wet period occurring during the Tauca (Heinrich 1) wet phase in the late Pleistocene [*Placzek et al.*, 2013] . SdA sedimentary records document variations in the hydrologic balance of SdAfrom >100 ka to present [*Bobst et al.*, 2001; *Godfrey et al.*, 2003; *Lowenstein et al.*, 2003]. Paleo-wetland deposits south of SdA suggest two wetter periods from 15.9–13.8 ka and 12.7–9.7 ka, (Central Andean Pluvial Event) [*Quade et al.*, 2008] consistent with vegetation records and wetland deposits throughout the region [*Betancourt et al.*, 2000; *Rech et al.*, 2002, 2003; *Quade et al.*, 2008]. Climate around SdA has been drier since the mid-Holocene based on the water table being below ground surface at paleo-wetland sites and observations from sediment cores at SdA [*Rech et al.*, 2002; *Quade et al.*, 2008; *Placzek et al.*, 2013]. The most recent period from 3.0 ka to present has been the driest since the late Pleistocene [e.g. *Betancourt et al.*, 2000].

2. Study Approach, Data Sources, and Methods

2.1 Conceptualization of the Modern Water Budget

Constraining the modern hydrologic budget is critical to evaluating whether the system is balanced within the topographic watershed. If the system is at steady state within the topographic watershed, groundwater recharge from precipitation (GW_{RCH}) plus surface water runoff (R) would balance all evapotranspiration (discharge) from SdA (D_{SdA}) with no change in storage (S). When considering the water budget beyond the topographic watershed one must also consider an additional loss term of evapotranspiration from salars and lakes in high elevation closed basins ($D_{HighElevSalars}$). The most conservative (more balanced) conceptualization of the modern hydrologic balance can be described by:

$$\Delta S = GW_{RCH} + R - D_{SdA} - D_{HighElevSalars} \qquad (1)$$

In the context of this equation, we provide uncertainty-bounded estimates of spatially distributed GW_{RCH} and $D_{HighElevSalars}$ throughout the region as the critically under-constrained term for assessing the hydrologic balance. A negative change in storage would suggest that water from outside the topographic basin or drawn from storage is needed to close the modern budget, whereas a positive change in storage would reflect recharge and surface water inputs currently outpacing evapotranspiration. We evaluate equation (1) for both the topographic watershed and the hydrogeologic watershed. We define the hydrogeologic watershed as the smallest potential contributing area within which the steady state hydrologic budget closes within reasonable uncertainty bounds (i.e. scenario M in *Corenthal et al.,* [2016]). This conservative scenario has the potential to double count some discharge in both the GW_{RCH} and R terms.

A less conservative (less balanced) water budget conceptualization assumes that baseflow in streams within the SdA watershed is sourced entirely from groundwater. In this conceptualization precipitation events recharge aquifers (GW_{RCH}), but do not generate runoff (R). This conceptualization of the modern hydrologic balance can be described by:

$$\boldsymbol{\Delta S = GW_{RCH} - D_{SdA} - D_{HighElevSalars}} \qquad (2)$$

Equation 2 does not include a surface water runoff term (R) and therefore yields a more negative estimate of change in groundwater storage. A more negative change in storage would suggest that even more water from outside the topographic watershed or drawn from storage is needed to close the modern water budget. These equations and the following budgets do not consider anthropogenic water extraction.

2.2 Precipitation

Precipitation estimates were obtained from the publicly-available Tropical Rainfall Measurement Mission (TRMM) 2B31 dataset of Mean Annual Precipitation (MAP) derived from 1–3 daily measurements at a resolution of 25 km^2. A processed TRMM 2B31 dataset was calibrated, validated, and provided by *Bookhagen and Strecker* [2008] over the period January 1, 1998 to December 31, 2009. This dataset was compared to gage measurements from 28 meteorological stations in the Region of Antofagasta maintained by the Chilean Dirección General de Aguas (DGA) and one station on the salar maintained by the Sociedad Chilena de Litio/Rockwood Lithium Inc./Albemarle (Figure S1 and S2). Power-law functions are fit to the lower and upper bound of the DGA station-TRMM data (Figure S2) to provide constraints on bias and uncertainty in the precipitation estimates. These bounds are used to estimate the median (most plausible), lower and upper ranges of MAP in the region and to provide a range of possible precipitation scenarios (Text S1). These ranges are incorporated in other dependent calculations below.

2.3 Groundwater Recharge

To determine GW_{RCH} from precipitation (P), we apply the chloride mass balance (CMB) method, which has been successfully applied to basins to the north and northwest of SdA [*Houston*, 2007, 2009], whereby

$$GW_{RCH} = \frac{P * Cl_p}{Cl_{gw} - Cl_{rw}} \qquad (3)$$

Where:

Cl_p = chloride concentration in precipitation

Cl_{gw} = chloride concentration in groundwater

Cl_{rw} = chloride contribution to groundwater from rock weathering

Common assumptions used in the application of the CMB method include (1) precipitation (P) is the only source of chloride (Cl^-) to groundwater, and (2) Cl^- is conservative in the groundwater system [*Bazuhair and Wood*, 1996]. Table 1 presents analyses of precipitation samples and locations.

We apply equation (3) to selected sample sites (Text S2) using the median, lower, and upper TRMM 2B31 derived P estimates [*Bookhagen and Strecker*, 2008] to determine a range of potential GW_{RCH} rates. A power function (Figure 3a) fit to the P and calculated GW_{RCH} is applied to the TRMM 2B31 datasets to generate lower, median, and upper estimate of the fraction of P than becomes GW_{RCH}. Estimates of GW_{RCH} were confined to areas that do not contain permanent discharge features (salars and lakes). The fraction of P that does not recharge groundwater is assumed to evapo-transpire or contribute to R. Herein, we pursue a conservative approach for closing the water budget and consider that R is generated by precipitation runoff (equation 1).

2.4 Evapotranspiration

Evapotranspiration (D_{SdA}) estimates from the nucleus and transition zone of SdA are summarized from works that (1) coupled eddy covariance station measurements taken in 2001 to remotely sensed land energy budgets (D_{SdA} range from 1.6–27.1 $m^{3/s}$) [*Kampf and Tyler*, 2006] and (2) coupled lysimeter measurements collected from 1983–1985 to land-type classifications from 1983–1985 (D_{SdA} of 5.6 $m^{3/s}$) [*Mardones*, 1986]. Of this range, we consider a maximum D_{SdA} of 22.7 m^3/s because higher estimates significantly over-predict fluxes from the nucleus [*Kampf and Tyler*, 2006]. We consider a minimum D_{SdA} of 5.6 m^3/s because it is the current estimate used to manage water resources of the basin [*Dirección General de Aguas*, 2013]. The infiltration rate determined through the CMB method is assumed to account for diffuse ET from anywhere not covered by a salar or lake.

Many closed basins above 3500 m in elevation host zones of focused evapotranspiration ($D_{HighElevSalars}$). Because no reliable $D_{HighElevSalars}$ measurements were available, a linear regression for potential ET (PET) (mm/year) as a function of ground elevation (m) for the Atacama region was used (Text S2).

2.5 Incorporation of Uncertainty in Hydrologic Balance Estimates

Each component of the water balance contains uncertainty that propagates through the calculations described above to consider a range of possible hydrologic balance estimates. At each stage of the calculations we consider these uncertainties and include them in final lower, median, and upper-end recharge scenarios which then are used to assess closure of the water budget. The precipitation amounts from TRMM impact both the precipitation-recharge CMB functional relationship (P in equation 3) as well as the assessed distributed recharge calculations. Additionally, uncertainty in the chloride composition (Cl_P in Equation 3) of the precipitation also impacts the effective recharge through the CMB calculation and functional relationship (equation 3). Our lower-end recharge estimates are calculated using the lowest possible precipitation estimates (Figure S2 – Upper Curve), the lowest precipitation chloride concentration, and omitting any Cl^- in groundwater sourced from rock weathering (Cl_{rw}). The median recharge estimate is produced using the TRMM 2B31 directly with the average chloride concentration in precipitation. Finally, the upper-end recharge estimates are calculated using highest possible precipitation estimates (Figure S2 – Lower Curve), the highest precipitation chloride concentration, and the possibility of Cl^- sourced from rock weathering.

3. Assessment and Uncertainty in the Hydrologic Balance

3.1 Precipitation

On the SdA salt flat annual precipitation averages 16 mm/year [*Sociedad Chilena de Litio Ltda.*, 2009], whereas >300 mm/year [*Bookhagen and Strecker*, 2008; *Quade et al.*, 2008] may occur above 5,000 m within the topographic watershed (Figure 1, Figure 3b). Approximately 50–80 mm/year of snow water equivalent occurs at 4500 m asl [*Vuille and Ammann*, 1997] but the majority likely sublimates before infiltrating [*Johnson et al.*, 2010; *Dirección General de Aguas*, 2013]. Based on the TRMM 2B31 dataset mean annual precipitation from 1998 to 2009, including the wetter than average 2001/2002, is 30.7 m^3/s (23.4 for lower bound and 51.7 m^3/s for upper bound) in recharge zones in the topographic watershed (Table 2), equivalent to a mean of 48 mm/year with a range of 0–340 mm/year (standard deviation of 45 mm/year). For the median precipitation scenario only 7% of the watershed area receives more than the 120 mm/year of precipitation threshold required for significant GW_{RCH} [*Scanlon et al.*, 2006; *Houston*, 2009] (Figure 3, Figure 4a), and most precipitation occurs above 3,500 m. Using this (median) scenario, infiltration rates of nearly 100% throughout the topographic watershed would be required to balance the highest estimates of D_{SdA}. .

3.2 Groundwater Recharge

Chloride concentration in precipitation samples ranged from 5–16 mg/L (Table 1). We combine our CMB results with those from the Turi and Linzor basins [*Houston*, 2007, 2009] to establish a new relationship for GW_{RCH} as a function of P (Figure 3) in this region. The range of chloride concentrations in precipitation bounds does not impact the fit of this function to the data, therefore we use a single relationship between precipitation and recharge (Text S3 and Figure S5). This relationship is fit using a power law with an R^2 of 0.82 as described:

$$GW_{RCH} = (1.3*10^{-4})*P^{2.3} \quad (4)$$

Applying equation (4) to the median TRMM 2B31 dataset predicts 1.1 m^3/s (1.1 for lower bound and 2.1 m^3/s for upper bound) of recharge within the topographic watershed (Figure 4b, Table 2), with infiltration rates ranging from 0.5–3.5% based on a precipitation Cl^- concentration of 8 mg/l, or 0.3–9.0% considering a range of precipitation Cl^- concentrations from 5–16 mg/l (Table 3, Figure 3). Similar to arid regions globally [*Scanlon et al.*, 2006] and the Central Andes [*Houston*, 2007], more than 1 mm/year of GW_{RCH} only occurs when precipitation exceeds 120 mm/year.

3.3 Evapotranspiration

Estimates of D_{SdA} range from 5.6–13.4 m^3/s [*Mardones*, 1986; *Kampf and Tyler*, 2006] (Table 2). We use a range of D_{SdA} estimates in our calculations, considering a minimum of 9.5 m^3/s based on the spatially variable latent heat flux method [*Kampf and Tyler*, 2006] and lysimeter study [*Mardones*, 1986]. We predict that $D_{HighElevSalars}$ in the hydrogeologic watershed totals 5.0 m^3/s (uncertainty range of 1.8–17.8 m^3/s) (Figure 4c, Table 2).

3.4 Surface Water and Shallow Groundwater Inflows

Approximately 3.19 m^3/s of shallow subsurface groundwater enters SdA (Corenthal et al. 2016; Munk et al., 2018). The *Direccion General de Aguas* [2013] estimates total streamflow to SdA is 1.58 m^3/s based on gage measurements, which alone matches our range of estimates of GW_{RCH} within the topographic watershed (1.1–2.1 m^3/s). The sum of shallow groundwater and streamflow (4.77 m^3/s) is consistent with but smaller than low estimates of D_{SdA} (5.6 m^3/s); however, GW_{RCH} within the topographic watershed accounts for only 24% of these inflows and only 5–20% of D_{SdA}. In order to balance the full range of discharge from evapotranspiration (5.6

to 13.4 m^3/s) with GW_{RCH} in the SdA topographic watershed, an average infiltration rate of 21 to 86 % is required. Such rates greatly exceed average infiltration rates for arid regions globally of 0.1–5% [*Scanlon et al.*, 2006] and infiltration rates observed in the Linzor and Turi basins [*Houston*, 2007, 2009].

3.5 Steady State Hydrologic Balance

Within the topographic watershed, D_{SdA} is 2–8 times (5.6–13.4 m^3/s) higher than the combined inputs of modern recharge from precipitation and streamflow (Figure 5; Table 2). Some streamflow is likely sourced from groundwater [e.g. *Hoke et al.*, 2004] and therefore counted twice, yielding more conservative estimates of hydrologic imbalance. The hydrogeologic watershed required for GW_{RCH}+R to balance evapotranspiration for our estimated range of recharge values has a surface area over 75,000 km^2, 4 times larger than the topographic watershed (Figure 5 scenario M). Even the high estimates of GW_{RCH}+R fail to explain the low estimates of D_{SdA} for watersheds A through I.

4. Closing the hydrologic budget

The modern hydrologic balance of the SdA topographic watershed does not close within reasonable uncertainty bounds (Table 2; Figure 5). We consider a range of uncertainties in the data including evapotranspiration estimates and bias in the TRMM 2B31 precipitation dataset correlation with gage data. To close this apparent hydrologic imbalance, the missing water could be explained by several sources [*Corenthal et al.*, 2016]. Here we explore two mechanisms to close the budget: (1) a larger watershed area that encompasses regional-scale inter-basin groundwater flow paths recharged from precipitation at higher elevations and (2) the modern hydrologic balance includes drainage of transient groundwater storage recharged during wetter conditions.

These two mechanisms are inferred to account for the majority of the missing water flux; however, additional flowpaths (e.g. orogenic groundwater) and systematic errors in ET and/or GW_{RCH} estimates could also explain portions of the imbalance. Infrequent, high-intensity precipitation events are known to rapidly recharge the groundwater system in areas where the water table is near the surface [*Boutt et al.,* 2016]. For the brine budget of SdA, such events are important to balance discharge from pumping and the low ET rates (<0.1 mm/year) in the halite aquifer. By applying equation 4 uniformly to the precipitation dataset, the potential for higher recharge rates in salars during intense rainfall is not included in the budget calculations. Nonetheless, the CMB method integrates over long-term timescales of recharge and accounts for these events in alluvium elsewhere in the Atacama [*Bazuhair and Wood*, 1996; *Houston*, 2006b]. Therefore, the CMB equation accounts for different types of freshwater recharge mechanisms

4.1 Steady state hydrologic system with residual water from regional groundwater flow (Mechanism 1)

The arid climate, high topographic relief and presence of laterally continuous permeable volcanic units dipping towards SdA support the potential for regional groundwater flow paths [*Tóth*, 1963; *Haitjema and Mitchell-Bruker*, 2005]. Within the proposed hydrogeologic watershed of 75,900 km ^{2}(Table 2; Figure 5 scenario M), GW_{RCH} + R balance evapotranspiration while maintaining an overall topographic gradient driving groundwater flow towards SdA; however, this watershed delineation is non-unique. Proposed recharge areas for many adjacent watersheds along the western Altiplano-Puna plateau margin overlap (Figure 5). We propose that regional groundwater flow plays an important role in the modern hydrologic balance of SdA; however, it likely cannot fully explain the observed discrepancy.

Inter-basin groundwater flow is assumed to occur in the central Andes [*Anderson et al.*, 2002; *Jordan et al.*, 2015], including the Monturaqui-Negrillar (MNT) aquifer that discharges in the southern SdA [*Rissmann et al.*, 2015]. To explain the existence of giant nitrate deposits in the Central Depression southwest and northwest of SdA, *Pérez-Fodich et al.* [2014] also suggest regional groundwater flowpaths. To the north, interbasin groundwater flow is necessary to close the hydrologic budget of the Río Loa catchment (drainage area = 33,570 km^2), where the Chilean DGA estimates a total of 6.4 m^3/s of water discharge [*Jordan et al.*, 2015], but we calculate only 1.6 – 4.0 m^3/s of GW_{RCH} within that topographic watershed. Using the plausible groundwater system of the Río Loa proposed by *Jordan et al.* [2015] (Figure 5); we estimate that approximately 8.5 – 14.3 m^3/s of GW_{RCH} occurs within this zone; however, this boundary overlaps with the major discharge zone of the Salar de Uyuni as well as a significant portion of our proposed hydrogeologic watershed for SdA. In order for these adjacent watersheds to have distinct recharge zones and be hydrologically balanced, it is apparent that some water must be drawn from transient storage.

4.2 Transient, draining groundwater storage (Mechanism 2)

Here we consider transient draining of groundwater storage to reconcile these budgets. We calculate the mean residence time of water [*Gelhar and Wilson*, 1974; *Lasaga and Berner*, 1998] within the SdA watershed is calculated to be 4.9 kyr using the conservative D_{SdA} rate of 5.6 m^3/s, an active aquifer thickness of 500 m, an area of 17,257 km^2 (i.e. area of the topographic watershed), and an effective porosity of 0.25. The dynamic response time [*Houston and Hart*, 2004] for the topographic watershed is 9.2 kyr and 42 kyr for the hydrogeologic watershed (Text S4). In systems with long residence and response times, the assumption that modern recharge rates must balance discharge rates is invalidated by having equilibration times greater than the timescale of documented climatic changes [*Currell et al.,* 2016]. High and low elevation groundwater age estimates lack a significant component of modern recharge further suggesting that these systems respond over long time scales [*Houston,* 2006b]. Evaporation at a smaller salar 50 km southwest of SdA exceeds modern recharge, and this imbalance has been explained by residual hydraulic head decay (i.e. groundwater storage) due to episodic recharge [*Houston and Hart*, 2004]. We now investigate these processes in a physically-based numerical model of a plateau-margin hydrogeologic system.

5 Numerical Simulations of a Plateau Margin Groundwater System

A transient 2-dimensional groundwater model simulating the Altiplano-Puna plateau and adjacent SdA system was constructed using the MODFLOW finite difference code for saturated flow [*McDonald and Harbaugh*, 1988]. The purpose of the model is to examine: (1) the dynamic response times of a regional groundwater system to changes in groundwater recharge that are of a magnitude similar to that predicted by paleoclimatic reconstructions [*Betancourt et al.*, 2000; *Placzek et al.*, 2013]; (2) the sensitivity of water level responses to these changes in groundwater recharge; and (3) whether the groundwater divide between water draining to SdA and water discharging to shallow basins on the plateau is dynamic or static with respect to changing recharge. The framework model is based on previous work in the Atacama by *Houston and Hart* [2004] and in the Murray Basin in Australia by *Urbano et al.*, [2004]. We evaluate this model for two scenarios of hydraulic conductivity that are designed to be conducive and restrictive to regional groundwater flowpaths; the conducive scenario is intended to approximate the northern half of SdA, and the restrictive scenario is intended to approximate the southern half of SdA. Together these scenarios represent the range of conditions expected along the plateau margin. Initial hydraulic head geometries were assigned based on the results of steady-state simulations, and the transient models simulate a period of 100,000 years (using 100 year timesteps) immediately following a step decrease in precipitation (recharge).

5.1 Base Model Geometry and Properties

The model domain is 250,000 m long (active domain of 219,200 m), unit width, and 3,000 m thick with grid dimensions of 200 m x 1 m x 200 m in the upper 7 layers and 200 m x 1 m x 400 m in the lower 4 layers. Elevations of the top grid cells were interpolated from a smoothed ASTER GDEM. The right, bottom and left faces of the model are no-flow boundaries. On the top boundary, there are 207 constant head cells in the upper layer at an elevation of 2300 m asl, representing the SdA surface. Specified flux boundaries were assigned to all other top cells. There are 119 drains along the plateau with conductance of 1,000 m^2/day. Along the plateau at an elevation of 3,893 m, 28 drains were assigned an elevation of 3,993 m and conductance of 10 $m^{2/}$day for the steady state run to produce a high elevation lake similar to those described by *Grosjean et al.* [1995], *Condom et al.*, [2004] and others. For the transient runs, the drains were assigned an elevation of 3,893m (top cell elevation) and conductance of 1,000 m^2/day to simulate a salar. Recharge was assigned to any top cell that was not already a drain or constant head boundary. For the initial steady-state simulations, recharge was determined by multiplying the TRMM 2B31 precipitation raster by a factor of three and applying equation 4 to this precipitation raster. This multiplication factor represents the upper (and conservative) estimates of precipitation during past pluvial periods in the most recent 130 ka [*Placzek et al.,* 2013]. This resultant raster was then interpolated to the model grid. For the transient run, modern GW_{RCH} rates were determined by applying equation 4 for GW_{RCH} to the modern TRMM 2B31 dataset and interpolating the resultant raster to the model grid. Interpolating the 3x modern precipitation and modern precipitation estimates for recharge inputs to the model captures the spatial distribution of GW_{RCH} across the plateau as well as the predicted relative magnitude of paleo- to modern- GW_{RCH} from the late Pleistocene to present based on *Betancourt et al.* [2000] and *Placzek et al.* [2013]. There are no other hydraulic sources or sinks in the model and the 2D model does not account for flow transverse to the domain, surface water features or direct precipitation runoff.

Two heterogeneous, isotropic hydraulic conductivity distributions were examined based on a geologic cross section through the SdA basin and the western Altiplano-Puna plateau by *Reutter et al.* [2006] (Figure 6). These scenarios are designed to represent: (1) southeastern SdA characterized by an uplifted, low permeability block of Precambrian to Carboniferous basement that interrupts the plateau margin (restrictive to regional flow) and (2) northeastern SdA characterized by monoclinal folding of laterally extensive ignimbrites (conducive to regional flow). Hydraulic conductivities for the geologic units described in *Reutter et al.* [2006] were assigned based on standard values from *Ingebritsen and Manning* [1999] and range from 0.01 to 10 m/day. For the transient simulations, a confined specific storage of 10^{-4} was assigned uniformly to the entire domain.

5.2 Model Results

5.2.1 Water Table Response to Changing Recharge Conditions

Water level responses to changing recharge conditions showed strong spatial variability with the most sensitivity observed in the area of the western and eastern plateau margins (Figure 7). Water levels showed a greater magnitude of response to recharge in the restrictive than in the conducive to regional flow simulations; however, the pattern of head decline was consistent between the models. In both simulations, less than 10 m of change in head was observed in cells within 7 km of a constant head cell at SdA throughout the 100,000 year simulation. Maximum head decline occurred near observation points 15 and 16, reaching 845 m of decline in the restrictive simulation and 370 m of decline in the conducive simulation. The magnitude of head decline increased with increasing elevation along the plateau margin. From west to east across the plateau, the magnitude of head decline decreased, reaching a minimum of 100 m decline by the high elevation drain cells for both simulations.

Figure 8 presents a comparison between modern and paleo hydraulic head observations in the conducive and restrictive cases. Observation points (see actual locations on Figure 5 and projected locations in Figure 7) are placed along corresponding model locations with modern and paleo- water table elevation estimates (Table S6). The two models are conceptual, and not specifically developed to match field observations, nonetheless, comparing results from the two models with field observations supports general interpretations and places first-order constraints on permeability structure of the plateau and plateau margin.

The pattern of modeled head declines is consistent with observed patterns inferred from paleoclimatic studies. During the Central Andean Pluvial Event in the late Pleistocene and early Holocene, paleowetland deposits and river incision records at elevations <3500 m show water table fluctuations on the scale of 1–25 m [e.g. *Betancourt et al.*, 2000; *Rech et al.*, 2002; *Quade et al.*, 2008], while lake levels and core records on the Altiplano-Puna plateau at elevations >3500 m show water table fluctuations of up to 130 m [*Grosjean et al.*, 1995; *Placzek et al.*, 2006, 2013]. In both modeled scenarios, after 10,000 years, the water table on the plateau margin at elevations <2,600 m declined by <25 m. The water table on the plateau near the discharge zone at elevations between 3880 m and 4120 m declined approximately 100 m by 10,000 years. No field observations of changes in water table are available on the plateau in areas distal to discharge zones.

5.2.2 Flow Budget Response Time to Changing Recharge

The ratio of flow out of the model from constant head cells on the salar surface and drains on the plateau margin (D_{SdA}) to total domain model recharge ($GW_{TotalRCH}$) is used as a metric to evaluate changes in the flow budget of the model over time. For all time steps of the 100,000 year transient simulation, GW_{RCH} was assigned modern values. This ratio is plotted as a function of simulation time in Figure 9. If the ratio of D_{SdA} to $GW_{TotalRCH}$ is greater than 1, then D_{SdA} must be supported in part by draining groundwater storage because the volume of water entering the salar exceeds total model recharge, where the fraction of discharging water supplied by draining storage is described by (D_{SdA}-$GW_{TotalRCH}$)/D_{SdA}. If D_{SdA}/$GW_{TotalRCH}$ equals 1, then D_{SdA} is entirely balanced by $GW_{TotalRCH}$ in the model domain, and no $GW_{TotalRCH}$ is discharging on the plateau. If D_{SdA}/$GW_{TotalRCH}$ is less than 1, then D_{SdA} is less than $GW_{TotalRCH}$ in the model domain and some fraction of $GW_{TotalRCH}$ is discharging from drains on the plateau ($D_{HIGHELEV}$).

For the restrictive to regional groundwater flow simulation, 60% of D_{SdA} is sourced from draining storage at t=100 years, and D_{SdA} is supplied entirely by $GW_{TotalRCH}$ after 19,200 years. For the conducive to regional groundwater flow simulation, 70% of D_{SdA} is sourced from draining storage at t=100 years, and D_{SdA} is supplied entirely by $GW_{TotalRCH}$ after 37,600 years. In the "conducive"simulation the water table on the plateau lies below the ground surface elevation and thus the elevation of the drains. For the "restrictive" simulation, $D_{SdA}/GW_{TotalRCH}$ is less than 1 for all times greater than 19,200 years. These results suggest that the low permeability zones must be present between the plateau and the basin floor to allow the high-elevation lakes and salars to exist.

If the change in $D_{SdA}/GW_{TotalRCH}$ between each time step is small, then the model has approached a steady state and the modeled system is adjusted to a reduction in groundwater recharge from 3x modern to modern. For the restrictive simulation, the dynamic response time is approximately 85,000 years, and approximately 38,000 years for the conducive simulation. These results are consistent with the dynamic response time calculations using general bulk aquifer properties of 42 kyr for the hydrogeologic watershed. The modeling results do not support the modern steady-state budget for systems with long response times.

5.2.3 Dynamic groundwater divides

Model results confirm that the groundwater divide separating water flowing to SdA and water discharging within the plateau do not coincide with topographic watershed boundaries (Figure 7 – vertical lines). In the initial steady state simulations for both scenarios, the groundwater divide occurs approximately 100 km from the easternmost constant head cell at SdA (or 50–70 km from the topographic divide). This length scale defines the upper distribution of flowpaths discharging at SdA. Once the transient simulation begins, the groundwater divide moves westward closer towards SdA as water is released from storage to augment discharge at SdA. In both simulations, after approximately 1,000 years, the groundwater divide reverses direction and begins to migrate eastward away from SdA as the volume of water released from storage decreases and regional groundwater recharge is captured. In the restrictive simulation, the position of the groundwater divide stabilizes by approximately 50,000–100,000 years around 130 km east of the easternmost constant head cell of SdA. In the conducive simulation, the groundwater divide reaches the easternmost boundary of the model after 9,000 years and does not move westward for the remainder of the simulation.

These results show that the groundwater divide of the plateau-margin system is dynamic at time scales similar to changes in climate and moves in response to changing recharge conditions. The position of the divide is also sensitive to presence of a lower conductivity block separating the discharge zone from the plateau, especially over longer time periods. While the "restrictive" case shows the greatest head change, it should be expected that groundwater divides along such portions of the plateau margin will be more stable over time than other segments of the plateau margin.

6. Discussion and Conclusions

The persistence and scope of questions relating to water imbalance in the Atacama Desert [e.g. *Magaritz et al.*, 1990; *Houston and Hart*, 2004; *Jordan et al.*, 2015], which is subject to high water resource demand for mining purposes, highlights the importance of better constraining groundwater divides and groundwater storage in these modern and paleo hydrologic systems. Observations of discharge along the Altiplano-Puna plateau margin greatly exceed our estimates of modern recharge rates to groundwater aquifers. In the absence of substantial overland flow this leaves an extreme hydrologic imbalance for catchments along the plateau margin.

The steady state assumption that recharge equals discharge is clearly not appropriate in this setting, despite its prevalence in the watershed management approaches throughout the region and globally. In order for recharge to equal discharge with hydrologic closure at steady state conditions, groundwater infiltration rates must be unrealistically high (15–24%; cf. *Scanlon et al.,* 2006). Recharge rates in basins to the east (Tuyajto; *Herrera, et al.* [2016]) and north (e.g. Pampa del Tamarugal; *Jayne et al.,* [2016]; and Salar de Huasco; Uribe et al., [2016]) using steady-state conditions are fundamentally flawed in the conceptualization of the sources of recharge water. Recharge during infrequent and sporadic precipitation events [*Boutt, et al.,* 2016; *Masbruch et al.,* 2016] could be a potential source of water but it must be explained in the context of recharge rates constrained using CMB estimates, which should reflect long-term average recharge rates.

Assuming that recharge water is moving from up-gradient closed basins requires a reorganization of how topographic boundaries are treated in the catchment hydrologic budgets as widely applied elsewhere [*Haitjema and Mitchell-Bruker,* 2005; *Gleeson et al.,* 2011]. Effort should be spent on identifying the hydrogeologic controls on the flowpaths of water and being able to distinguish this regional groundwater from local groundwater inputs using elemental, isotopic, and molecular tracers. In the case of regional steady state flow towards these basins, shallow hydraulic heads should show strong downward gradients and should have equipotentials that lower in magnitude towards the basins. Both of these conditions have significant implications for the water budget of the high elevation (> 4000 m) closed basins on the plateau. The water budget of these basins should be negative with some fraction of water flowing out of the basin to neighboring basins. One nearby basin, Laguna Tuayito shows that this is case [*Herrera et al.,* 2016]. Secondly, water levels in these basin floors are likely perched above a regional water table. Both considerations have strong implications for lake-based precipitation paleo-climate reconstruction. Reconstructions assume that lake levels in the closed basin respond solely to precipitation minus evaporation. If one were to assume losses of water between basins or out the basin bottom to the regional groundwater table, it would lead to an underestimate of precipitation in the region. Basins that receive substantial groundwater input from another would lead to an overestimate of precipitation. Understanding the magnitude of hydraulic losses through infiltration from perched basins above a regional water table is critical.

By coupling solute and water budgets, additional constraints may be gained. *Corenthal et al.* [2016] demonstrated that the modern sodium (Na) flux to the SdA basin could account for the halite and brine deposits over ~10 Ma, consistent with geological constraints. If the Na concentration of inflow water is assumed to be constant over this interval, the long-term average discharge rates are also required to remain relatively constant. Both the water molecule and any conservative solutes must achieve mass balance in a realistic conceptualization of the hydrologic system. Therefore, agreement in water and solute budgets is strong support for a realistic and reasonable hydrologic model. Similarly, recharge area and transient storage can be constrained by solute budgets. Although this is outside the scope of this manuscript, we suggest that the yield of weathering derived solutes per unit area must fall within the range observed for arid montane catchments globally to justify the size of the hydrogeologic watershed. Additionally, solute release rates from groundwater systems must match the modeled draining of transient storage and predicted mean residence times for groundwater. In the case where such constraints cannot be reconciled, a reconceptualization of the hydrogeologic model will require adjustments that effect any combination of the following: (1) the scale of regional groundwater flow, (2) the mean residence time of water, and (3) the potential for deep, under-sampled flowpaths.

Our present conceptualization of the extreme modern hydrologic imbalance along the western margin of the Altiplano-Puna plateau can be explained by a combination of regional groundwater flow and transient draining of groundwater storage. Transient draining of groundwater storage is required because presumed recharge areas for many watersheds at the plateau margin overlap. Dynamic groundwater flow modeling suggests: (1) the water level changes at the salar margins (and discharging water to fans) are highly sensitive to changes in recharge on plateau, (2) the extent and magnitude of the changes in hydraulic head are controlled by the distribution of hydraulic conductivity at the plateau margin, (3) the contributing area to SdA changes, is not coincident with the topographic boundary, and is a dynamic feature, and (4) it is difficult to reconcile the modern position of the "water table" on the plateau with the regional groundwater flow conceptualization and the modern discharge to SdA (i.e., modern salars are perched and lose water to surrounding basins and ultimately to SdA and adjacent plateau margin catchments).

The hydrologic imbalance at SdA has important implications for paleoclimatic reconstructions, implying that paleo-lakes on the Altiplano lost water to SdA altering their hydrologic budgets and further complicating lake-level based paleoclimatic reconstructions. Because water resources of SdA are managed under the steady state assumption, these findings have implications for efforts to sustainably allocate water resources for mining, agricultural and environmental interests. Such considerations apply to many continental settings with strong gradients in landscape and climate, though the margins of large orogenic plateau are likely to exhibit the greatest hydrologic imbalance by virtue of their scale.

7. Acknowledgments

The authors would like to acknowledge Rockwood Lithium, Inc./Albemarle Corporation for their continued support of this and related research to improve the understanding of the hydrogeology and geochemistry of the SdA environment. The ASTER DEM and Landsat 8 OLI were retrieved from EarthExplorer, courtesy of the NASA Land Processes Distributed Active Archive Center, USGS/Earth Resources Observation and Science Center. Processed and calibrated TRMM 2B31 dataset, a joint mission between NASA and the Japan Aerospace Exploration Agency, was kindly made publically accessible by B. Bookhagen.

8. References

Alley, W. M., R. W. Healy, J. W. LaBaugh, and T. E. Reilly (2002), Flow and storage in groundwater systems., Science, 296(5575), 1985–1990, doi:10.1126/science.1067123.

Andermann, C., L. Longuevergne, S. Bonnet, A. Crave, P. Davy, and R. Gloaguen (2012), Impact of transient groundwater storage on the discharge of Himalayan rivers, Nat. Geosci., 5(2), 127–132, doi:10.1038/ngeo1356.

Anderson, M., R. Low, and S. Foot (2002), Sustainable groundwater development in arid, high Andean basins, Geol. Soc. London, Spec. Publ., 193(1), 133–144, doi:10.1144/GSL.SP.2002.193.01.11.

Aron, F., G. González, E. Veloso, and J. Cembrano (2008), Architecture and style of compressive Neogene deformation in the eastern-southeastern border of the Salar de Atacama Basin (22°30'-24°15'S): A structural setting for the active volcanic arc of the Central Andes, Int. Symp. Andean Geodyn., (1998), 52–55.

Bazuhair, A. S., and W. W. Wood (1996), Chloride mass-balance method for estimating ground water recharge in arid areas: Examples from western Saudi Arabia, J. Hydrol., 186(1-4), 153–159, doi:10.1016/S0022-1694(96)03028-4.

Betancourt, J. L., C. Latorre, J. A. Rech, J. Quade, and K. A. Rylander (2000), A 22,000-Year Record of Monsoonal Precipitation from Northern Chile's Atacama Desert, Science (80-.)., 289(5484), 1542–1546, doi:10.1126/science.289.5484.1542.

Blodgett, T. a., J. D. Lenters, and B. L. Isacks (1997), Constraints on the origin of paleolake expansions in the Central Andes, Earth Interact., 1(1), 1–1, doi:10.1175/1087-3562(1997)001<0001:CotOoP>2.0.CO;2.

Bobst, A. L., T. K. Lowenstein, T. E. Jordan, L. V. Godfrey, T. L. Ku, and S. Luo (2001), A 106 ka paleoclimate record from drill core of the Salar de Atacama, northern Chile, Palaeogeogr. Palaeoclimatol. Palaeoecol., 173(1-2), 21–42, doi:10.1016/S0031-0182(01)00308-X.

Bookhagen, B., and M. R. Strecker (2008), Orographic barriers, high-resolution TRMM rainfall, and relief variations along the eastern Andes, Geophys. Res. Lett., 35(6), 1–6, doi:10.1029/2007GL032011.

Boutt D. F., Hynek S. A., Munk L. A., and Corenthal L. G. (2016) Rapid recharge of fresh water to the halite-hosted brine aquifer of Salar de Atacama, Chile, Hydrol. Process., 30: 4720–4740. doi: 10.1002/hyp.10994.

Cervetto Sepulveda, M. M. (2012), Caracterización hidrogeológica e hidrogeoquímica de las cuencas: Salar de Aguas Calientes 2, Puntas Negras, Laguna Tuyajto, Pampa Colorada, Pampa las Tecas y Salar el Laco, II Region de Chile [M.S. Thesis], Universidad de Chile.

Condom, T., A. Coudrain, A. Dezetter, D. Brunstein, F. Delclaux, and S. Jean-Emmanuel (2004), Transient modelling of lacustrine regressions: two case studies from the Andean Altiplano, Hydrol. Process., 18(13), 2395–2408, doi:10.1002/hyp.1470.

Condon, L. E., and R. M. Maxwell (2015), Evaluating the relationship between topography and groundwater using outputs from a continental-scale integrated hydrology model, Water Resour. Res., 51, 6602–6621, doi:10.1002/2014WR016774.

Corenthal, L. G., D. F. Boutt, S. A. Hynek, and L. A. Munk (2016), Regional groundwater flow and accumulation of a massive evaporite deposit at the margin of the Chilean Altiplano, Geophys. Res. Lett., 43, doi:10.1002/2016GL070076

Craig, H. (1961), Isotopic Variations in Meteoric Waters., Science, 133(3465), 1702–3, doi:10.1126/science.133.3465.1702.

Crossey, L. J., T. P. Fischer, P. J. Patchett, K. E. Karlstrom, D. R. Hilton, D. L. Newell, P. Huntoon, A. C. Reynolds, and G. a. M. de Leeuw (2006), Dissected hydrologic system at the Grand Canyon: Interaction between deeply derived fluids and plateau aquifer waters in modern springs and travertine, Geology, 34(1), 25, doi:10.1130/G22057.1.

Currell, M., Gleeson, T., & Dahlhaus, P. (2016). A new assessment framework for transience in hydrogeological systems. *Groundwater,* 54(1), 4–14.

Dirección General de Aguas (2013), Análisis de la Oferta Hídrica del Salar de Atacama, Santiago, Chile.

Dunai, T. J., G. a. González López, and J. Juez-Larré (2005), Oligocene-Miocene age of aridity in the Atacama Desert revealed by exposure dating of erosion-sensitive landforms, Geology, 33(4), 321–324, doi:10.1130/G21184.1.

Fritz, S. C., P. a. Baker, T. K. Lowenstein, G. O. Seltzer, C. a. Rigsby, G. S. Dwyer, P. M. Tapia, K. K. Arnold, T. L. Ku, and S. Luo (2004), Hydrologic variation during the last 170,000 years in the southern hemisphere tropics of South America, Quat. Res., 61(1), 95–104, doi:10.1016/j.yqres.2003.08.007.

Garreaud, R., M. Vuille, and A. C. Clement (2003), The climate of the Altiplano: Observed current conditions and mechanisms of past changes, Palaeogeogr. Palaeoclimatol. Palaeoecol., 194(1-3), 5–22, doi:10.1016/S0031-0182(03)00269-4.

Gayo, E. M., C. Latorre, T. E. Jordan, P. L. Nester, S. A. Estay, K. F. Ojeda, and C. M. Santoro (2012), Late Quaternary hydrological and ecological changes in the hyperarid core of the northern Atacama Desert (~21°S), Earth-Science Rev., 113(3-4), 120–140, doi:10.1016/j.earscirev.2012.04.003.

Gelhar, L. W. & Wilson, J. L. Ground-Water Quality Modeling. *Ground Water* **12,** 399–408 (1974).

Gorelick, S. M., and C. Zheng (2015), Global change and the groundwater management challenge, Water Resour. Res., 51, 3031–3051, doi:10.1002/2014WR016825.

Gleeson, T., L. Marklund, L. Smith, and A. H. Manning (2011), Classifying the water table at regional to continental scales, Geophys. Res. Lett., 38(5), 1–6, doi:10.1029/2010GL046427.

Gleeson, T., Y. Wada, M. F. P. Bierkens, and L. P. H. van Beek (2012), Water balance of global aquifers revealed by groundwater footprint, Nature, 488(7410), 197–200, doi:10.1038/nature11295.

Godfrey, L. V., T. E. Jordan, T. K. Lowenstein, and R. L. Alonso (2003), Stable isotope constraints on the transport of water to the Andes between 22o and 26oS during the last glacial cycle, Palaeogeogr. Palaeoclimatol. Palaeoecol., 194(1-3), 299–317, doi:10.1016/S0031-0182(03)00283-9.

Grosjean, M., M. A. Geyh, B. Messerli, and U. Schotterer (1995), Late-glacial and early Holocene lake sediments, ground-water formation and climate in the Atacama Altiplano 22°24'S, J. Paleolimnol., 14(3), 241–252, doi:10.1007/BF00682426.

Haitjema, H. M., and S. Mitchell-Bruker (2005), Are Water Tables a Subdued Replica of the Topography?, Ground Water, 43(6), 781–786, doi:10.1111/j.1745-6584.2005.00090.x.

Hartley, A. J., and G. Chong (2002), Late Pliocene age for the Atacama Desert: Implications for the desertification of western South America, Geology, 30(1), 43–46, doi:10.1130/0091-7613(2002)030<0043:LPAFTA>2.0.CO;2.

Herrera Lameli, C. (2011), Informe Final Estudio Hidrogeologico Proyecto " Planta de Sulfato de Cobre Pentahidratado ," , 0–33.

Herrera, C. et al., 2016. Groundwater flow in a closed basin with a saline shallow lake in a volcanic area: Laguna Tuyajto, northern Chilean Altiplano of the Andes. Science of the Total Environment, 541, p.303-318.

Hoke, G. D., B. L. Isacks, T. E. Jordan, and J. S. Yu (2004), Groundwater-sapping origin for the giant quebradas of northern Chile, Geology, 32(7), 605–608, doi:10.1130/G20601.1.

Houston, J. (2006a), Evaporation in the Atacama Desert: An empirical study of spatio-temporal variations and their causes, J. Hydrol., 330(3-4), 402–412, doi:10.1016/j.jhydrol.2006.03.036.

Houston, J. (2006b), The great Atacama flood of 2001 and its implications for Andean hydrology, Hydrol. Process., 20(3), 591–610, doi:10.1002/hyp.5926.

Houston, J. (2007), Recharge to groundwater in the Turi Basin, northern Chile: An evaluation based on tritium and chloride mass balance techniques, J. Hydrol., 334(3-4), 534–544, doi:10.1016/j.jhydrol.2006.10.030.

Houston, J. (2009), A recharge model for high altitude, arid, Andean aquifers, Hydrol. Process., 23(16), 2383–2393, doi:10.1002/hyp.7350.

Houston, J., and D. Hart (2004), Theoretical head decay in closed basin aquifers: an insight into fossil groundwater and recharge events in the Andes of northern Chile, Quat. J. Eng. Geol. Hydrogeol., 37(December 2007), 131–139, doi:10.1144/1470-9236/04-007.

Ingebritsen SE, Manning CE (1999) Geological implications of a permeability-depth curve for the continental crust. Geology, 27, 1,107–10.

Jayne, R. S., R. M. Pollyea, J. P. Dodd, E. J. Olson, and S. K. Swanson (2016), Spatial and temporal constraints on regional-scale groundwater flow in the Pampa del Tamarugal Basin, Atacama Desert, Chile, *Hydrogeol. J.*, (August), 1921–1937, doi:10.1007/s10040-016-1454-3.

Johnson, E., J. Yáñez, C. Ortiz, and J. Muñoz (2010), Evaporation from shallow groundwater in closed basins in the Chilean Altiplano, Hydrol. Sci. J., 55(4), 624–635, doi:10.1080/02626661003780458.

Jordan, T., C. Herrera Lameli, N. Kirk-Lawlor, and L. Godfrey (2015), Architecture of the aquifers of the Calama Basin, Loa catchment basin, northern Chile, Geosphere, 11(5), GES01176.1, doi:10.1130/GES01176.1.

Jordan, T. E., N. Munoz, M. Hein, T. Lowenstein, L. Godfrey, and J. Yu (2002a), Active faulting and folding without topographic expression in an evaporite basin, Chile, Bull. Geol. Soc. Am., 114(11), 1406–1421, doi:10.1130/0016-7606(2002)114<1406:AFAFWT>2.0.CO;2.

Jordan, T. E., L. V. Godfrey, N. Munoz, R. N. Alonso, T. K. Lowenstein, G. D. Hoke, N. Peranginangin, B. L. Isacks, and L. Cathles (2002b), Orogenic-scale ground water circulation in teh Central Andes: evidence and consequences., 5th ISAG (International Symp. Andean Geodyn., 331–334.

Jordan, T. E., C. Mpodozis, N. Muñoz, N. Blanco, P. Pananont, and M. Gardeweg (2007), Cenozoic subsurface stratigraphy and structure of the Salar de Atacama Basin, northern Chile, J. South Am. Earth Sci., 23(2-3), 122–146, doi:10.1016/j.jsames.2006.09.024.

Kampf, S. K., and S. W. Tyler (2006), Spatial characterization of land surface energy fluxes and uncertainty estimation at the Salar de Atacama, Northern Chile, Adv. Water Resour., 29(2), 336–354, doi:10.1016/j.advwatres.2005.02.017.

Lamb, S., and P. Davis (2003), Cenozoic climate change as a possible cause for the rise of the Andes., Nature, 425(6960), 792–797, doi:10.1038/nature02049.

Lasaga, A. C. & Berner, R. A. Fundamental aspects of quantitative models for geochemical cycles. *Chem. Geol.* **145,** 161–175 (1998).

Lowenstein, T. K., and F. Risacher (2009), Closed basin brine evolution and the influence of Ca–Cl inflow waters: Death Valley and Bristol Dry Lake California, Qaidam Basin, China, and Salar de Atacama, Chile, Aquat. Geochem., 15, 71–94, doi:10.1007/s10498-008-9046-z.

Lowenstein, T. K., M. C. Hein, A. L. Bobst, T. E. Jordan, T.-L. Ku, and S. Luo (2003), An Assessment of stratigraphic completeness in climate-sensitive closed-basin lake sediments: Salar de Atacama, Chile, J. Sediment. Res., 73(1), 91–104, doi:10.1306/061002730091.

Magaritz, M., R. Aravena, H. Pena, O. Suzuki, and A. Grilli (1990), Source of ground water in the deserts of Northern Chile: Evidence of deep circulation of ground water from the Andes, Ground Water, 28(4), 513–517, doi:10.1111/j.1745-6584.1990.tb01706.x.

Mardones, L. (1986), Características geológicas e hidrogeológicas del Salar de Atacama, in El litio: Un nuevo recurso para Chile, edited by G. Lagos, pp. 181–216, Universidad de Chile, Santiago, Chile.

Martínez, F., López, C., Bascuñan, S., & Arriagada, C. (2018). Tectonic interaction between Mesozoic to Cenozoic extensional and contractional structures in the Preandean Depression (23°–25°S): Geologic implications for the Central Andes. Tectonophysics, 744, 333–349. https://doi.org/10.1016/j.tecto.2018.07.016

Masbruch, M. D., C. A. Rumsey, S. Gangopadhyay, D. D. Susong, and T. Pruitt (2016), Analyses of infrequent (quasi-decadal) large groundwater recharge events in the northern Great Basin: Their importance for groundwater availability, use, and management, Water Resour. Res., 52, doi:10.1002/2016WR019060.

Maxwell, P. (2014), Analysing the lithium industry: Demand, supply, and emerging developments, Miner. Econ., 26(3), 97–106, doi:10.1007/s13563-013-0041-5.

McDonald, M. G., and A. W. Harbaugh (1988), A modular three-dimensional finite-difference ground-water flow model, United States Geological Survey.

McGuire, K. J., and J. J. McDonnell (2010), Hydrological connectivity of hillslopes and streams: Characteristic time scales and nonlinearities, Water Resour. Res., 46, W10543, doi:10.1029/2010WR009341.

McNamara, J. P., D. Tetzlaff, K. Bishop, C. Soulsby, M. Seyfried, N. E. Peters, B. T. Aulenbach, and R. Hooper (2011), Storage as a metric of catchment comparison, Hydrol. Processes, 25, 3364–3371.

Montgomery, E. L., M. J. Rosko, S. O. Castro, B. R. Keller, and P. S. Bevacqua (2003), Interbasin underflow between closed Altiplano basins in Chile., Ground Water, 41(4), 523–31.

Munk, L.A., Hynek, S.A., Bradley, D.C., Boutt, D.F., Labay, K., Jochens, H., 2016. Lithium Brines: A Global Perspective, *in* Verplanck, P.L. and Hitzman, M.W., eds., Rare Earth and Critical Elements in Ore Deposits. *Reviews in Economic Geology* (18), 339–365.

Munk, L. A., Boutt, D. F., Hynek, S. A., & Moran, B. J. (2018). Hydrogeochemical fluxes and processes contributing to the formation of lithium-enriched brines in a hyper-arid continental basin. Chemical Geology, 493, 37–57. https://doi.org/10.1016/j.chemgeo.2018.05.013

Muñoz, Enrique, Álvarez, César, Billib, Max, Arumí, José Luis, & Rivera, Diego. (2011). Comparison of Gridded and Measured Rainfall Data for Basin-scale Hydrological Studies. Chilean journal of agricultural research, 71(3), 459-468. doi: 10.4067/S0718-58392011000300018

Nelson, S.T., Anderson, K.W., and Mayo, A.L., 2004, Testing the interbasin flow hypothesis at Death Valley, CA, USA: Eos, v. 85, p. 349, 355-356.

Nelson, S.T., and Mayo, A.L., 2014, The role of interbasin groundwater transfers in geologically complex terranes, demonstrated by the Great Basin in the western United States: Hydrogeology Journal, v. 22, p. 807-822, DOI 10.1007/s10040-014-1104-6.

Pérez-Fodich, A., M. Reich, F. Álvarez, G. T. Snyder, R. Schoenberg, G. Vargas, Y. Muramatsu, and U. Fehn (2014), Climate change and tectonic uplift triggered the formation of the atacama desert's giant nitrate deposits, Geology, 42(3), 251–254, doi:10.1130/G34969.1.

Placzek, C., J. Quade, and P. J. Patchett (2006), Geochronology and stratigraphy of late Pleistocene lake cycles on the southern Bolivian Altiplano: Implications for causes of tropical climate change, Bull. Geol. Soc. Am., 118(5-6), 515–532, doi:10.1130/B25770.1.

Placzek, C. J., J. Quade, and P. J. Patchett (2013), A 130ka reconstruction of rainfall on the Bolivian Altiplano, Earth Planet. Sci. Lett., 363, 97–108, doi:10.1016/j.epsl.2012.12.017.

Quade, J., J. a. Rech, J. L. Betancourt, C. Latorre, B. Quade, K. A. Rylander, and T. Fisher (2008), Paleowetlands and regional climate change in the central Atacama Desert, northern Chile, Quat. Res., 69(3), 343–360, doi:10.1016/j.yqres.2008.01.003.

Ramirez, C., and M. Gardeweg (1982), Carta Geologica de Chile, escala 1:250000, Hoja Toconao, Region de Antofagasta, Chile No. 54, Santiago, Chile.

Rech, J. a, J. L. Betancourt, and J. Quade (2002), Late Quaternary paleohydrology of the central Atacama Desert (lat 22 -24 S), Chile, Geol. Soc. Am. Bull., 114(3), 334–348, doi:10.1130/0016-7606(2002)114<0334:LQPOTC>2.0.CO;2.

Rech, J. a., J. S. Pigati, J. Quade, and J. L. Betancourt (2003), Re-evaluation of mid-Holocene deposits at Quebrada Puripica, northern Chile, Palaeogeogr. Palaeoclimatol. Palaeoecol., 194, 207–222, doi:10.1016/S0031-0182(03)00278-5.

Reutter, K.-J. et al. (2006), The Salar de Atacama Basin : A Subsiding block within the western edge of the Altiplano-Puna Plateau, Andes. Act. Subduction Orogeny, 303–325.

Risacher, F., H. Alonso, and C. Salazar (2003), The origin of brines and salts in Chilean salars: A hydrochemical review, Earth-Science Rev., 63(3-4), 249–293, doi:10.1016/S0012-8252(03)00037-0.

Rissmann, C., M. Leybourne, C. Benn, and B. Christenson (2015), The origin of solutes within the groundwaters of a high Andean aquifer, Chem. Geol., 396, 164–181, doi:10.1016/j.chemgeo.2014.11.029.

Rubilar, J., Martínez, F., Arriagada, C., Becerra, J., 2017. Structure of the Cordillera de la Sal: A key tectonic element for the Oligocene-Neogene evolution of the Salar de Atacama basin, Central Andes, northern Chile. J. S. Am. Earth Sci. https://doi.org/10.1016/j.jsames.2017.11.013.

Salas, J., J. Guimerà, O. Cornellà, R. Aravena, E. Guzmán, C. Tore, W. Von Igel, and R. Moreno (2010), Hidrogeología del sistema lagunar del margen este del Salar de Atacama (Chile), Bol. Geol. y Min., 121(4), 357–372.

Salisbury, M. J., B. R. Jicha, S. L. de Silva, B. S. Singer, N. C. Jiménez, and M. H. Ort (2011), 40Ar/39Ar chronostratigraphy of Altiplano-Puna volcanic complex ignimbrites reveals the development of a major magmatic province, Bull. Geol. Soc. Am., 123(5), 821–840, doi:10.1130/B30280.1.

Scanlon, B. R., K. E. Keese, A. L. Flint, L. E. Flint, C. B. Gaye, W. M. Edmunds, and I. Simmers (2006), Global synthesis of groundwater recharge in semiarid and arid regions, Hydrol. Process., 20(15), 3335–3370, doi:10.1002/hyp.6335.

Schaller, M. F., and Y. Fan (2009), River basins as groundwater exporters and importers: Implications for water cycle and climate modeling, J. Geophys. Res. Atmos., 114(4), doi:10.1029/2008JD010636.

Sociedad Chilena de Litio Ltda. (2009), Informe Hidrología e Hidrogeología Adenda 1 - EIA Modificaciones y Mejoramiento del Sistema de Pozas de Evaporación Solar en el Salar de Atacama, Antofagasta, Chile.

Tóth, J. (1963), A theoretical analysis of groundwater flow in small drainage basins, J. Geophys. Res., 68(16), 4795–4812, doi:10.1029/JZ068i016p04795.

Tyler, S. W., J. F. Muñoz, and W. W. Wood (2006), The response of playa and sabkha hydraulics and mineralogy to climate forcing, Ground Water, 44(3), 329–338, doi:10.1111/j.1745-6584.2005.00096.x.

Urbano, I. D., M. Person, K. Kelts, and J. S. Hanor (2004), Transient groundwater impacts on the development of paleoclimatic lake records in semi-arid environments, Geofluids, 4(3), 187–196, doi:10.1111/j.1468-8123.2004.00081.x.

Uribe, J., Muñoz, J.F., Gironás, J. Oyarzún, R., Aguirre, E. and Aravena, R. (2016) Assessing groundwater recharge in an Andean closed basin using isotopic characterization and a rainfall-runoff model: Salar del Huasco basin, Chile, Hydrogeology Journal 23 (7), 1535-1551

van Beek, L. P. H., Y. Wada, and M. F. P. Bierkens (2011), Global monthly water stress: 1. Water balance and water availability, Water Resour. Res., 47, W07517, doi:10.1029/2010WR009791

Vuille, M., and C. Ammann (1997), Regional snowfall patterns in the high, arid Andes, Clim. Change, 36, 413–423, doi:10.1007/978-94-015-8905-5_10.

Ward, K. M., G. Zandt, S. L. Beck, D. H. Christensen, and H. McFarlin (2014), Seismic imaging of the magmatic underpinnings beneath the Altiplano-Puna volcanic complex from the joint inversion of surface wave dispersion and receiver functions, Earth Planet. Sci. Lett., 404, 43–53, doi:10.1016/j.epsl.2014.07.022.

FIGURE CAPTIONS:

Figure 1: Locator map and cross-section of elevation and precipitation for the SdA region of 21 to 25° S. (a) Elevations (0 to > 6,000 m) from an Advanced Spaceborne Thermal Emission and Reflection Radiometer (ASTER) Global Digital Elevation Model (GDEM). Gages maintained by the Chilean DGA. (b) ASTER GDEM derived elevation and TRMM 2B31 estimates of MAP from 1998 to 2009.

Figure 2: (a) Stable isotopic composition of samples considered for CMB calculations. Samples collected as part of this study and from *Cervetto* [2012]. Only samples of inflow groundwater from wells in alluvial fans that plot closely to the global meteoric water line, shown as solid black diamonds, were selected for the CMB calculations. (b) Stable isotopic composition of groundwater samples within the topographic watershed used for CMB analysis. CMB cutoff is deuterium excess <5 $^{o}/_{oo}$.

Figure 3 Results of chloride mass balance (CMB). (a) GWR determined by the CMB method based on samples in the SdA, Linzor basin and Chilean Puna Plateau. Uncertainty includes a range of Cl in precipitation from 5–16 mg/l. MAP from the TRMM 2B31 dataset. Solid line is the best fit to calculated CMB results, while the dashed line shows the infiltration rate required to close the steady state hydrologic budget in the SdA topographic watershed. (b) Frequency distribution of gridded (25 km^2) MAP from the TRMM 2B31 dataset within the topographic watershed.

Figure 4 Spatial distribution of P, GWR for the median precipitation scenario and PET used to evaluate the topographic and regional scale hydrologic budget of the SdA. (a) MAP from 1998–2009 based on TRMM 2B31 dataset. Black circles are groundwater Cl sample locations. (b) Median annual GWR from 1998-2009 determined by applying equation (2) to median precipitation dataset. (c) PET determined as a function of elevation applied to discharge zones (gray polygons), excluding SdA.

Figure 5 A) Regional watersheds from Corenthal et al. (2016) for the evaluation the steady state contributing regions for the Salar de Atacama and Rio Loa Basins using full uncertainty considerations for the water balance. Each lettered zone for SdA includes the cumulative area of all smaller zones. A is the topographic watershed, and M is the inferred hydrogeologic watershed where GWR+R balances ET in the full uncertainty bounds. The Rio Loa contributing areas are from Jordan et al. (2015). Background is an ASTER DEM. Dashed line indicates the position of the 2-D model presented in Figure 6. Numbered locations refer to modern and paleo hydraulic head estimates in Figures 7 and 8. B) Chloride mass balance recharge + runoff estimates (blue diamonds) for lower (light blue) and upper bound recharge (dark blue) scenarios. Evapotranspiration bounds (red diamonds) for lower (light red) and upper estimates (dark red). Letters indicate the areas represented by the black polygons in A).

Figure 6 Model geometry, boundary conditions, hydraulic conductivity distribution, and initial water table positions for the restrictive and conducive simulations described in text.

Figure 7: Simulated hydraulic head distributions for (A) restrictive and (B) conducive simulations at time of 0, 1000, 10000, 100000 years after change in recharge. Position of the hydrogeologic divides are shown for labeled times in vertical black lines. Numbered locations correspond to head observations locations plotted in Figure 8.

Figure 8 Simulated hydraulic heads (y-axis) for restrictive and conducive simulations compared to modern field and paleo-hydraulic head estimates (x-axis). Sizes of colored polygons (pink – conducive, blue – restrictive) are based on simulated heads with the highest position being the initial condition for the models. Highest observed heads are estimated based on paleo-hydrologic information cited in text and presented in Supporting Information 5.

Figure 9 Plot of the ratio of discharge from constant head cells at SdA and drains along the plateau margin (D_{SdA}) to specified total model recharge ($GW_{TOTALRCH}$). The un-shaded region represents discharge to SdA that is greater than total model recharge (i.e. some contribution of groundwater storage). The shaded represents times in the simulation where discharge to SdA is less than the total model recharge.

TABLE CAPTIONS:

Table 1: Locations and characteristics of precipitation samples used to determine chloride concentrations in precipitation

Table 2: Predicted precipitation and recharge for topographic and hydrogeologic catchments

Table 1: Tabulated attributes and results of groundwater chloride analyses including estimates of groundwater recharge from the CMB method.

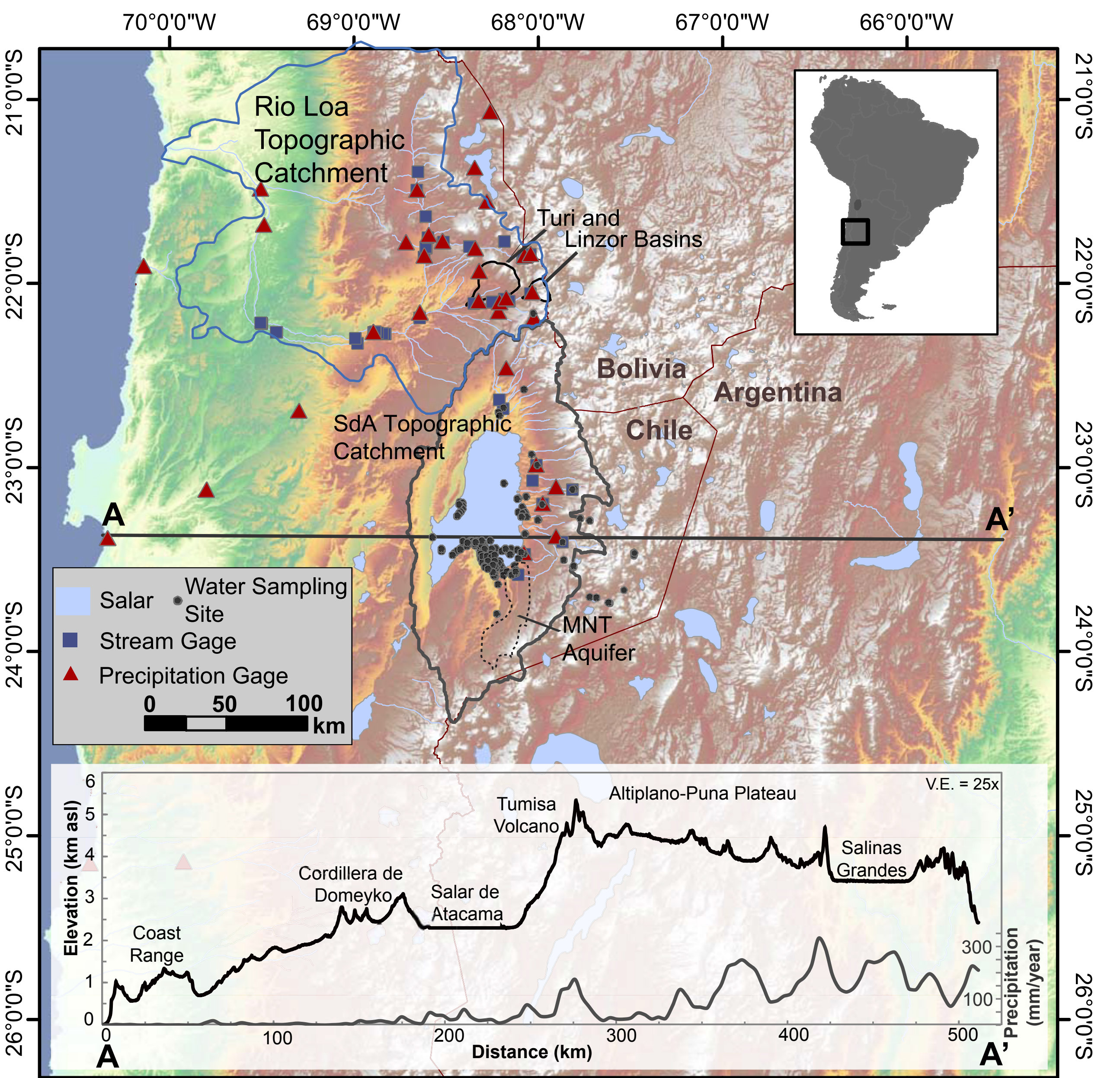

Figure 1: Locator map and cross-section of elevation and precipitation for the SdA region of 21 to 25° S. (a) Elevations (0 to > 6,000 m) from an Advanced Spaceborne Thermal Emission and Reflection Radiometer (ASTER) Global Digital Elevation Model (GDEM). Gages maintained by the Chilean DGA. (b) ASTER GDEM derived elevation and TRMM 2B31 estimates of MAP from 1998 to 2009.

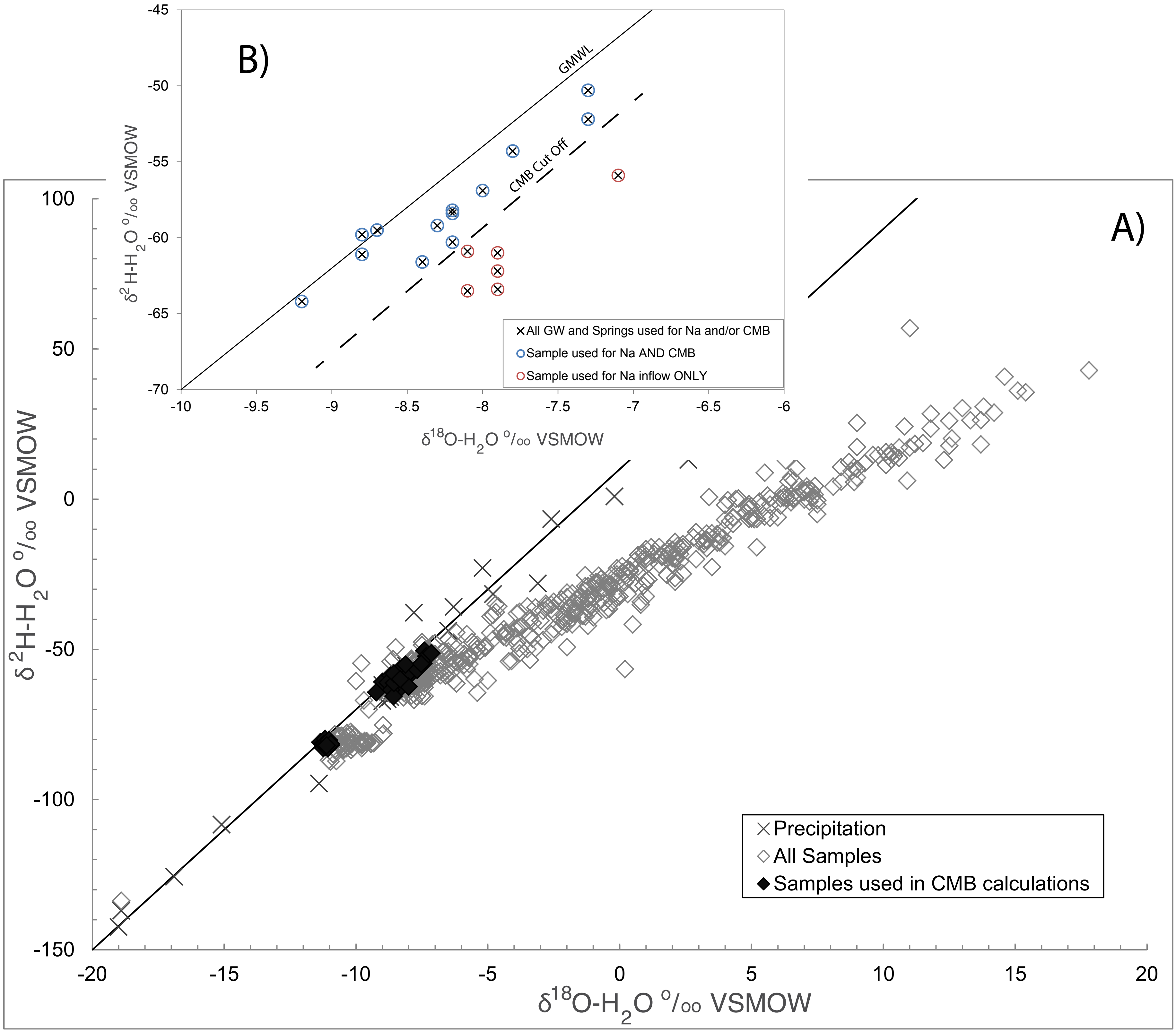

Figure 2: (a) Stable isotopic composition of samples considered for CMB calculations. Samples collected as part of this study and from Cervetto [2012]. Only samples of inflow groundwater from wells in alluvial fans that plot closely to the global meteoric water line, shown as solid black diamonds, were selected for the CMB calculations. (b) Stable isotopic composition of groundwater samples within the topographic watershed used for CMB analysis. CMB cutoff is deuterium excess <5 $^{o}/_{oo}$.

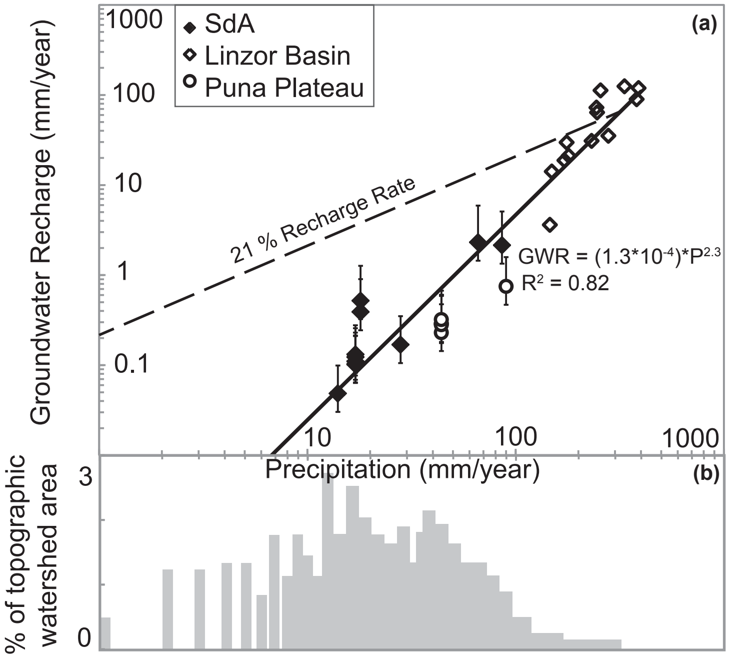

Figure 3 Results of chloride mass balance (CMB). (a) GWR determined by the CMB method based on samples in the SdA, Linzor basin and Chilean Puna Plateau. Uncertainty includes a range of Cl in precipitation from 5–16 mg/l. MAP from the TRMM 2B31 dataset. Solid line is the best fit to calculated CMB results, while the dashed line shows the infiltration rate required to close the steady state hydrologic

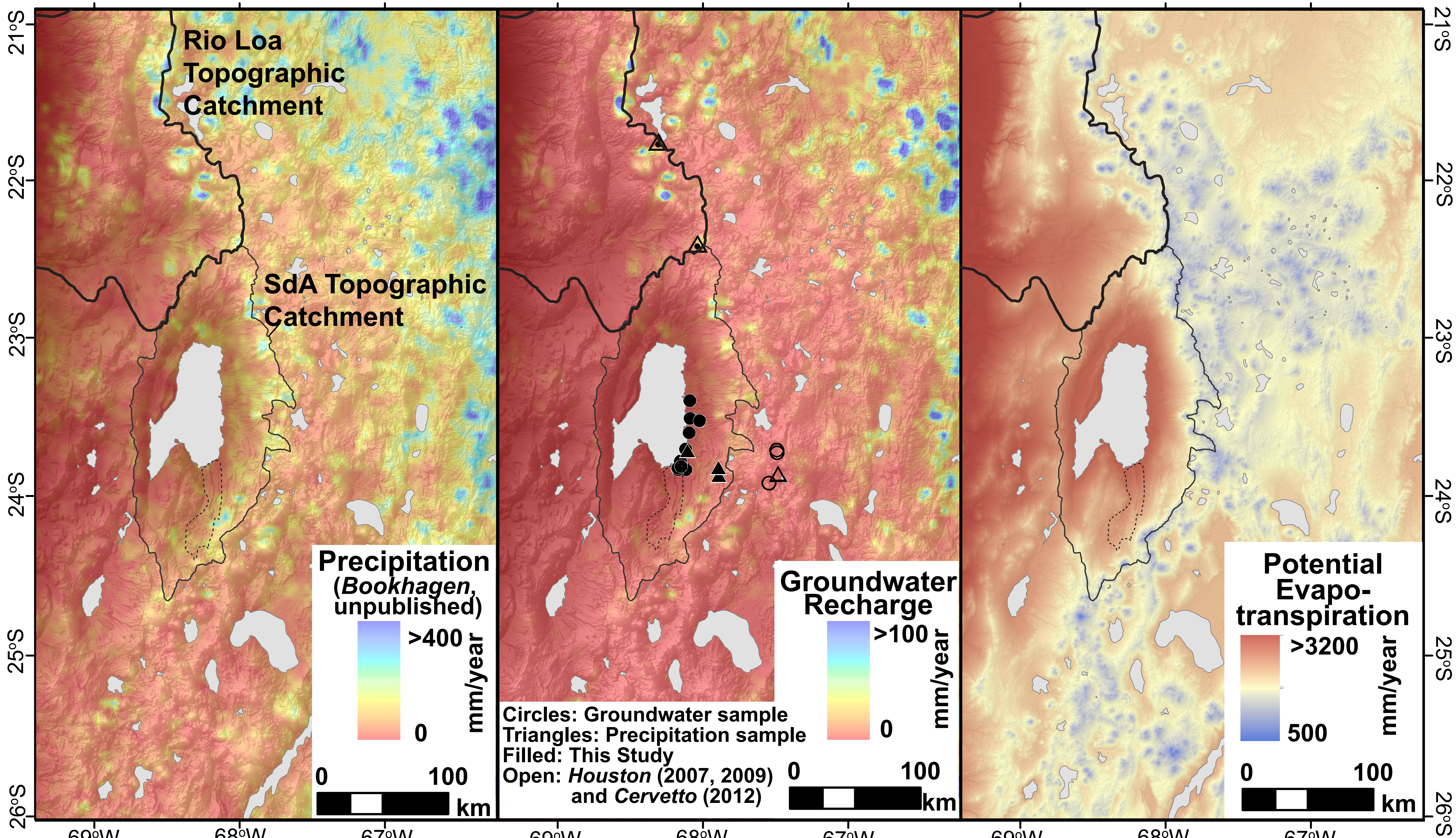

Figure 4 Spatial distribution of P, GWR for the median precipitation scenario and PET used to evaluate the topographic and regional scale hydrologic budget of the SdA. (a) MAP from 1998–2009 based on TRMM 2B31 dataset. Black circles are groundwater Cl sample locations. (b) Median annual GWR from 1998-2009 determined by applying equation (2) to median precipitation dataset. (c) PET determined as a function of elevation applied to discharge zones (gray polygons), excluding SdA.

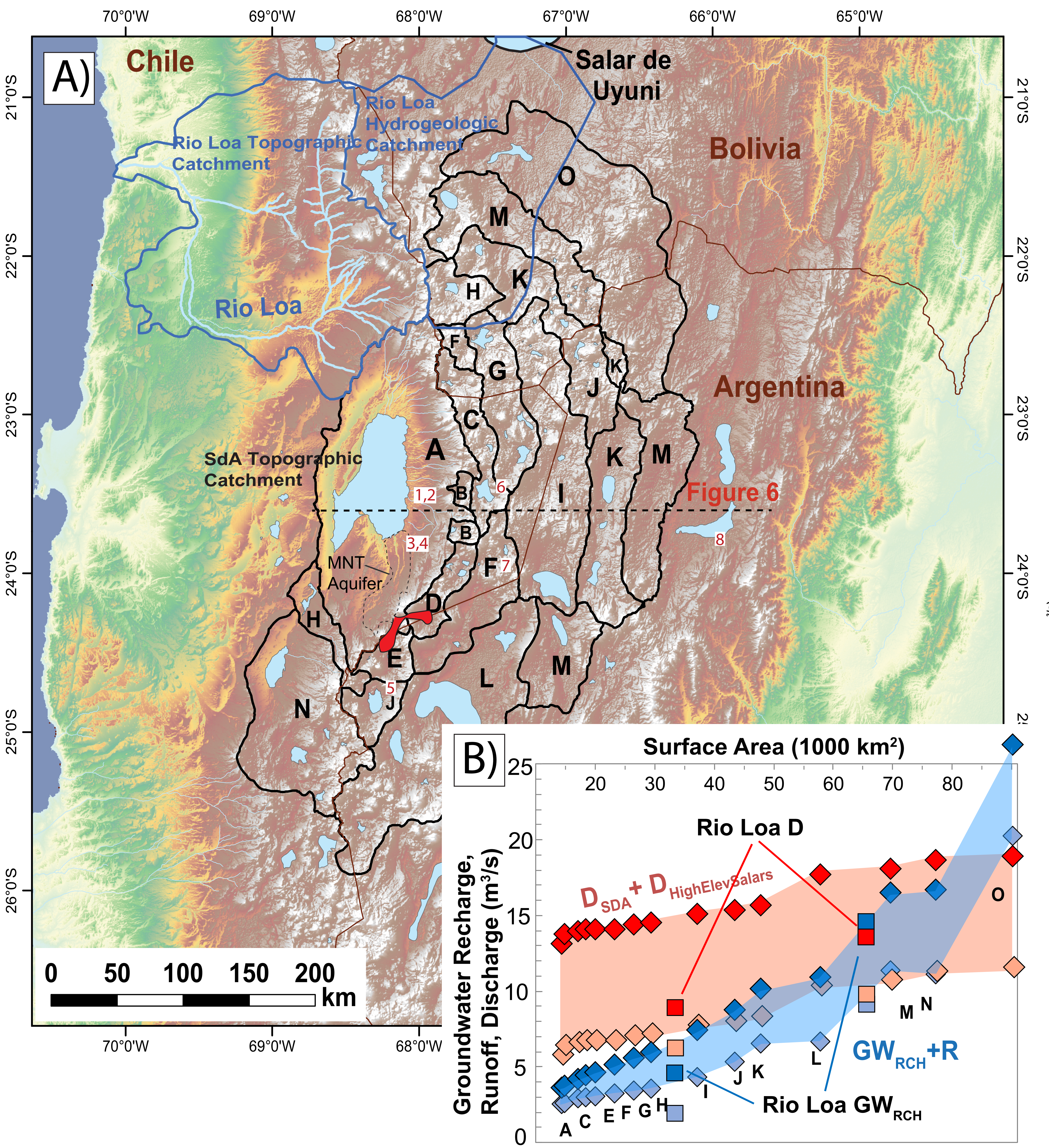

Figure 5 A) Regional watersheds from Corenthal et al. (2016) for the evaluation the steady state contributing regions for the Salar de Atacama and Rio Loa Basins using full uncertainty considerations for the water balance. Each lettered zone for SdA includes the cumulative area of all smaller zones. A is the topographic watershed, and M is the inferred hydrogeologic watershed where GWR+R balances ET in the full uncertainty bounds. The Rio Loa contributing areas are from Jordan et al. (2015). Background is an ASTER DEM. Dashed line indicates the position of the 2-D model presented in Figure 6. Numbered locations refer to modern and paleo hydraulic head estimates in Figures 7 and 8. B) Chloride mass balance recharge + runoff estimates (blue diamonds) for lower (light blue) and upper bound recharge (dark blue) scenarios. Evapotranspiration bounds (red diamonds) for lower (light red) and upper estimates (dark red). Letters indicate the areas represented by the black polygons in A).

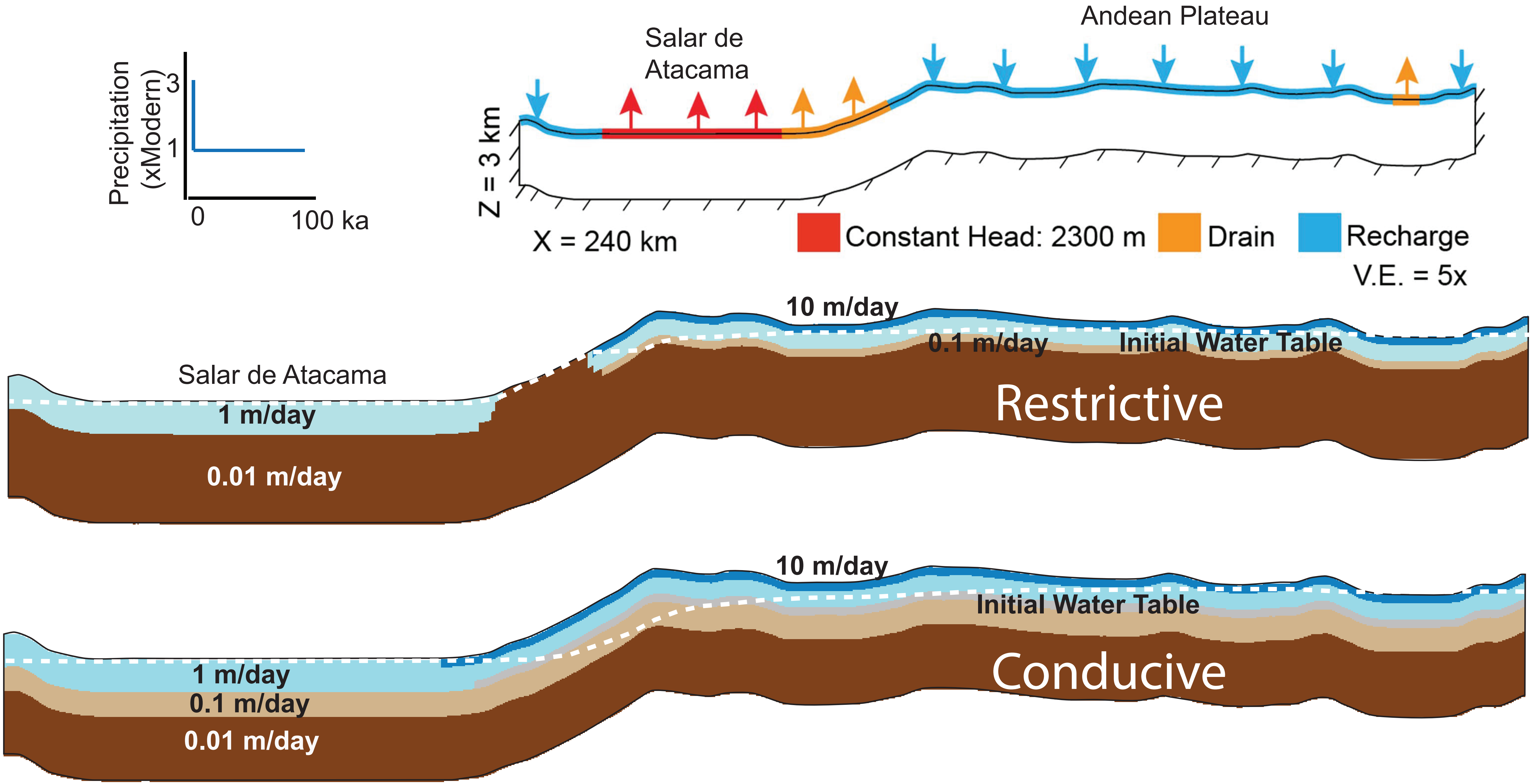

Figure 6 Model geometry, boundary conditions, hydraulic conductivity distribution, and initial water table positions for the restrictive and conducive simulations described in text.

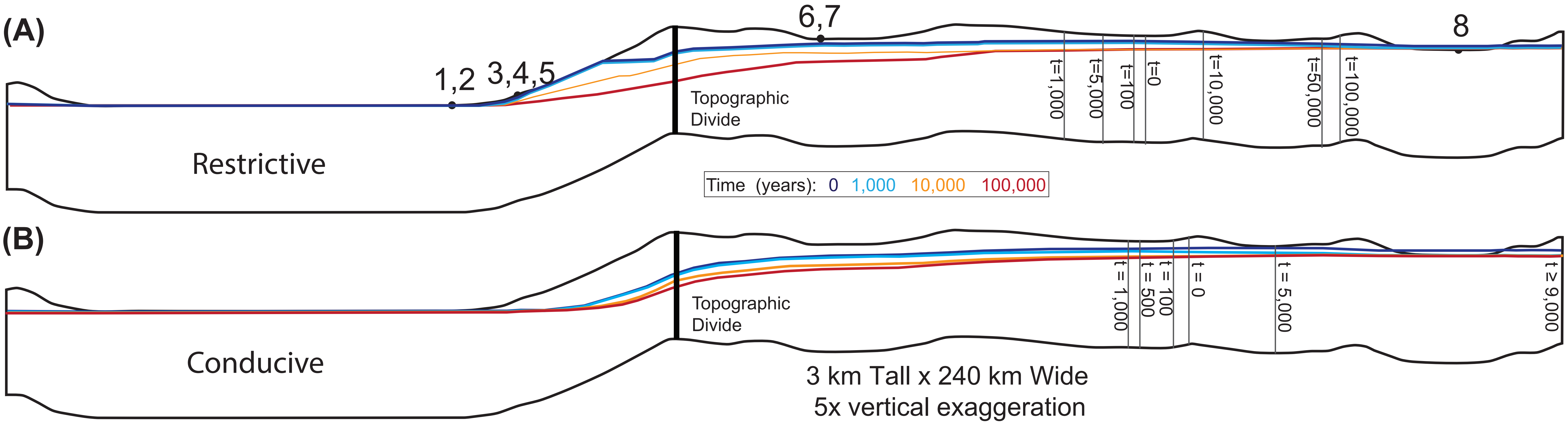

Figure 7: Simulated hydraulic head distributions for (A) restrictive and (B) conducive simulations at time of 0, 1000, 10000, 100000 years after change in recharge. Position of the hydrogeologic divides are shown for labeled times in vertical black lines. Numbered locations correspond to head observations locations plotted in Figure 8.

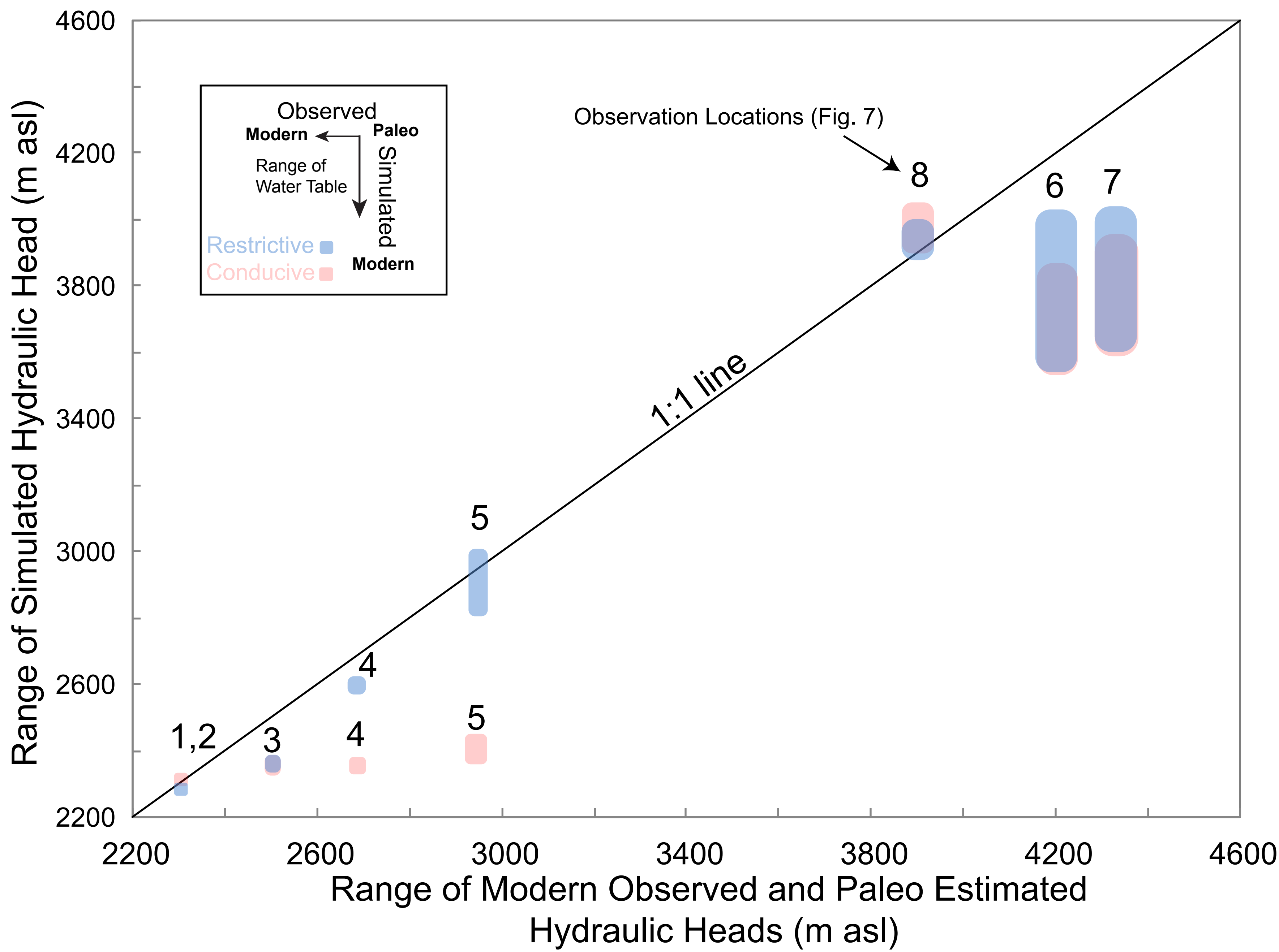

Figure 8 Simulated hydraulic heads (y-axis) for restrictive and conducive simulations compared to modern field and paleo-hydraulic head estimates (x-axis). Sizes of colored polygons (pink – conducive, blue – restrictive) are based on simulated heads with the highest position being the initial condition for the models. Highest observed heads are estimated based on paleo-hydrologic information cited in text and presented in Supporting Information 5.

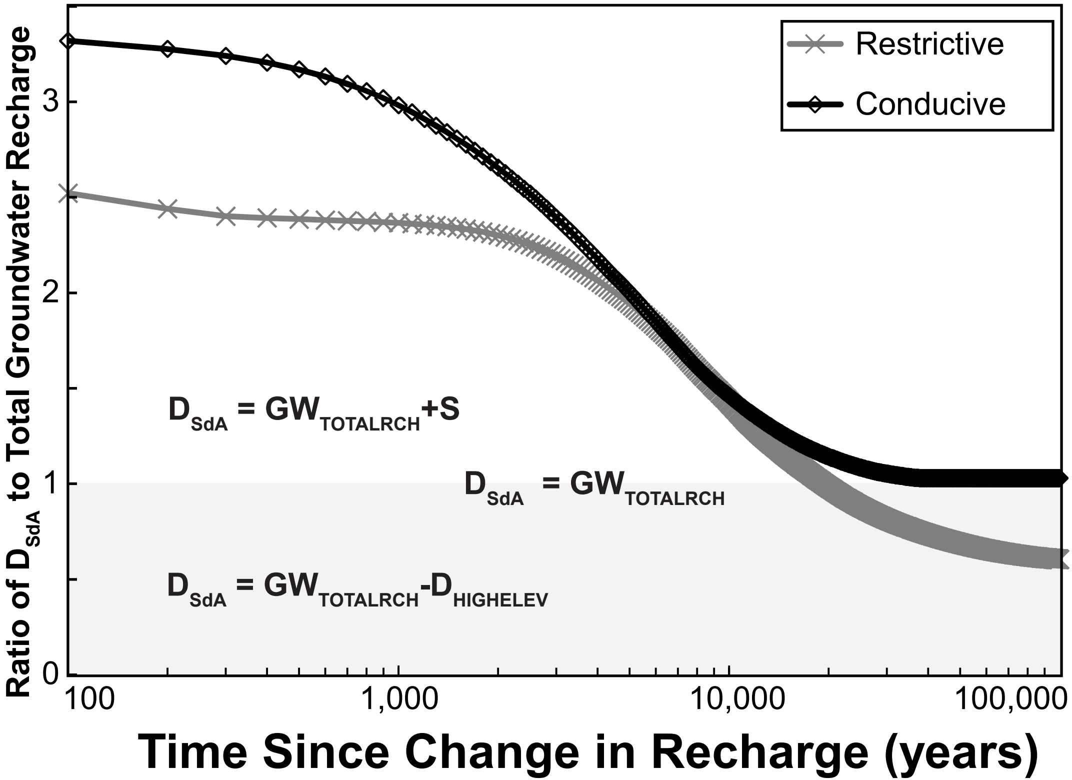

Figure 9 Plot of the ratio of discharge from constant head cells at SdA and drains along the plateau margin (DSdA) to specified total model recharge (GWTOTALRCH). The un-shaded region represents discharge to SdA that is greater than total model recharge (i.e. some contribution of groundwater storage). The shaded represents times in the simulation where discharge to SdA is less than the total model recharge.

Table 1: Locations and characteristics of precipitation samples used to determine chloride concentrations in precipitatio

Sample ID	Date	Longitude	Latitude	Elevation	Cl	$\delta^{18}O$	$\delta^{2}H$	Reference
		WGS84		m asl	mg/l	‰ VSMOW		
SDA185W	41293	-67.8534	-23.8374	3940	9.6	-16.9	-125.7	N/A
SDA190W	41411	-68.0673	-23.6818	2381	8.1	-18.9	-137.0	N/A
SDA220W	41655	-67.8549	-23.7876	3825	15.8	-2.6	-6.6	N/A
LAC.P001	38718	-67.4450	-23.8281	4307	<10	-18.0	-135.4	Cervetto, 2012
Ascotan	1999-2000	-68.27	-21.72	3956	28	ND	ND	Houston, 2007
Colchane	1999-2000	-68.65	-19.28	3965	10	ND	ND	Houston, 2007
Collacagua	1999-2000	-68.83	-20.05	3990	4	ND	ND	Houston, 2007
El Tatio	1999-2000	-68	-22.37	4345	5	ND	ND	Houston, 2007

Table 2: Predicted Precipitation and Recharge for Topographic and Hydrogeologic Catchments

		Topographic Watershed	**Hydrogeologic Watershed**
Total Surface Area (km^2)		17257	75924
Area of Recharge Zones (km^2)		14319	69676
Precipitation	(P)	30.7 (23.4-51.7)	199.4 (171.4-284.4)
Recharge from precipitation	(GWR)	1.1 (1.1-2.1)	10.0 (9.7-14.6)
Surface water inflow	(R)	1.6 (0.5-2)	1.6 (0.5-2)
Evapotranspiration from SdA	(ET_{SdA})	9.5 (5.6-13.4)	9.5 (5.6-13.4)
Evapotranspiration from higher elevation salars	($ET_{HighElevSalars}$)	0	5.0 (1.8-17.8)
ΔStorage	(ΔS)	-6.8 (-11.8--1.5)	-2.9 (-21.0-+9.2)

Table 3: Tabulated attributes and results of groundwater chloride analyses including estimates of groundwater recharge fro

Site ID	**Long.**	**Lat.**	**Elev.**	**Approx. Depth to Water**	**Date**	**Cl_{gw}**	**Na_{gw}**	**$\delta^{18}O$**	**$\delta^{2}H$**	**D-ex**	**P**	**GWR**	**GWR/P**
	WGS84		m asl	m		mg/l	mg/l	‰ VSMOW			mm/year	mm/year	%
SDA139W	-67.988	-23.495	2568	Spring	Average	320.9	222.7	-8.0	-56.9	7.4	86	2.1 (1.3-5.1)	2.5 (1.6-5.9)
					4/3/12	*207.7*	*231.8*	*-8.3*	*-60.0*				
					9/24/12	*201.9*	*220.5*	*-7.7*	*-56.8*				
					1/11/13	*555.3*	*225.1*	*-7.5*	*-54.8*				
					5/19/13	*311.6*	*224.0*	*-8.1*	*-55.1*				
					1/17/14	*327.9*	*212.0*	*-8.6*	*-58.0*				
SDA140W	-68.050	-23.476	2340	18.5	Average	277.3	217.0	-8.2	-60.3	5.3	18	0.5 (0.3-1.3)	2.9 (1.8-7.0)
					4/3/12	*224.8*	*210.9*	*-8.0*	*-62.4*				
					9/24/12	*366.5*	*215.6*	*-8.4*	*-63.3*				
					1/11/13	*319.9*	*238.2*	*-8.1*	*-58.7*				
					5/19/13	*197.9*	*203.2*	*-8.3*	*-56.6*				
SDA161W	-68.112	-23.771	2338	23.4	Average	1579.7	913.0	-7.8	-54.3	8.2	15	0.1 (0-0.2)	0.5 (0.3-1.0)
					9/29/12	*1650.2*	*1075.0*	*-7.6*	*-54.6*				
					1/12/13	*1745.9*	*904.9*	*-7.8*	*-54.2*				
					1/13/13	*1732.7*	*779.4*	*-7.9*	*-53.8*				
					5/14/13	*1949.4*	*904.9*	*-7.8*	*-54.2*				
					1/14/14	*1525.9*	*1001.9*	*-8.0*	*-55.9*				
					8/18/14	*873.8*	*811.9*	*-7.9*	*-53.1*				
SDA186W	-67.985	-23.491	2574	21.7	Average	228.5	215.4	-8.2	-58.2	7.4	66	2.3 (1.4-5.9)	3.5 (2.2-9.0)
					1/19/13	*231.3*	*220.1*	*-7.9*	*-57.9*				
					5/19/13	*225.7*	*210.8*	*-8.5*	*-58.5*				
SDA226W	-68.137	-23.794	2329	13.3	Average	1339.9	768.5	-7.3	-50.3	8.3	17	0.1 (0.1-0.2)	0.6 (0.4-1.2)
					1/19/14	*1457.5*	*811.6*	*-7.5*	*-52.2*				
					8/18/14	*1222.3*	*725.5*	*-7.1*	*-48.3*				
SDA227W	-68.134	-23.800	2338	25.2	Average	1032.3	621.5	-8.7	-59.5	9.9	17	0.1 (0.1-0.3)	0.8 (0.5-1.6)
					1/19/14	*842.1*	*686.9*	*-8.6*	*-58.0*				
					8/18/14	*1222.6*	*556.1*	*-8.8*	*-60.9*				
SDA228W	-68.136	-23.789	2335	11.6	Average	1107.7	705.5	-8.8	-59.8	10.9	17	0.1 (0.1-0.3)	0.7 (0.5-1.5)
					1/19/14	*948.0*	*711.2*	*-9.0*	*-60.8*				
					8/18/14	*1267.4*	*699.8*	*-8.7*	*-58.8*				
SDA229W	-68.118	-23.746	2313	4.7	1/19/14	1232.9	882.3	-8.8	-61.1	9.3	17	0.1 (0.1-0.2)	0.6 (0.4-1.4)
SDA2W	-68.081	-23.671	2333	15	Average	1328.4	782.6	-7.3	-52.2	6.4	28	0.2 (0.1-0.4)	0.6 (0.4-1.3)
					9/30/11	*1983.3*	*696.2*	*-7.7*	*-56.2*				
					1/12/12	*1097.1*	*718.6*	*-8.7*	*-63.4*				
					4/8/12	*1414.2*	*798.8*	*-8.6*	*-65.6*				
					9/26/12	*819.0*	*916.8*	*-8.6*	*-61.2*				
SDA76W	-68.053	-23.365	2387	43.6	Average	369.0	340.3	-7.3	-52.2	6.5	18	0.4 (0.2-0.9)	2.2 (1.4-5.0)
					1/13/12	*354.2*	*301.1*	*-7.3*	*-52.2*				
					4/3/12	*370.6*	*365.1*	*-7.5*	*-54.7*				
					1/11/13	*382.9*	*341.9*	*-7.1*	*-51.3*				
					5/19/13	*368.4*	*353.1*	*-7.4*	*-50.5*				
SDA84W	-68.057	-23.569	2329	9.9	Average	2309.2	1460.1	-8.2	-58.4	7.0	14	0.0 (0-0.1)	0.3 (0.2-0.7)
					1/14/12	*2214.0*	*1446.5*	*-8.3*	*-59.3*				
					4/7/12	*2830.9*	*1620.1*	*-8.2*	*-60.5*				
					9/24/12	*2197.2*	*1334.5*	*-8.2*	*-59.6*				
					5/19/13	*2042.3*	*1284.0*	*-7.9*	*-56.2*				
					1/11/13	*2259.0*	*1722.3*	*-8.2*	*-56.2*				
					1/9/14	*2312.0*	*1353.2*	*-8.3*	*-58.7*				
SDA85W	-68.114	-23.780	2351	23.1	Average	1632.6	958.5	-8.3	-59.2	7.1	15	0.1 (0-0.2)	0.5 (0.3-1.0)
					1/14/12	*1527.8*	*921.6*	*-8.3*	*-60.5*				
					4/8/12	*1867.5*	*1048.1*	*-8.3*	*-62.5*				
					9/25/12	*1576.7*	*1000.4*	*-8.4*	*-62.4*				
					1/12/13	*1668.3*	*957.3*	*-8.2*	*-57.6*				
					5/14/13	*1483.7*	*852.0*	*-8.2*	*-55.8*				
					1/9/14	*1671.4*	*971.4*	*-8.3*	*-56.5*				
SDA8AW	-68.109	-23.791	2373	Spring	1/9/14	1323.1	867.0	-9.2	-64.2	9.6	17	0.1 (0.1-0.2)	0.6 (0.4-1.3)
COL.T008.1	-67.507	-23.885	4261	No Data	Average	960.0	652.0	-11.3	-81.1	9.3	90	0.8 (0.5-1.6)	0.9 (0.5-1.8)
					10/30/08	*994.3*	*692.0*	*-11.2*	*-81.2*				
					10/30/08	*925.6*	*612.0*	*-11.4*	*-80.9*				
PN.T005.1	-67.451	-23.676	4376	31.1	Average	1220.0	0.0	-11.0	-81.5	6.6	44	0.3 (0.2-0.6)	0.7 (0.4-1.4)
					11/26/04	*1250.0*	*0.0*	*-11.0*	*-80.2*				
					11/26/04	*1220.0*	*0.0*	*-10.9*	*-81.4*				
					11/27/04	*1190.0*	*0.0*	*-11.1*	*-82.9*				
PN.T006.1	-67.451	-23.693	4364	44.4	11/27/04	1220.0	0.0	-11.1	-82.0	6.9	44	0.3 (0.2-0.6)	0.7 (0.4-1.4)
PN.T007.6	-67.452	-23.692	4361	No Data	Average	1533.3	593.3	-11.2	-81.7	7.8	44	0.2 (0.1-0.5)	0.5 (0.3-1.1)
					9/1/05	*1510.0*	*593.0*	*-11.2*	*-79.8*				
					1/16/05	*1540.0*	*597.0*	*-11.2*	*-82.8*				
					1/20/05	*1550.0*	*590.0*	*-11.2*	*-82.5*				
PN.T008.2	-67.453	-23.677	4374	52.89	Average	1250.0	434.7	-11.1	-81.8	7.2	44	0.3 (0.2-0.6)	0.6 (0.4-1.3)
					12/22/04	*1260.0*	*425.0*	*-11.2*	*-81.4*				
					1/16/05	*1240.0*	*442.0*	*-11.2*	*-82.0*				
					1/20/05	*1250.0*	*437.0*	*-11.0*	*-81.9*				
PN.T014	-67.449	-23.678	4383	No Data	10/29/08	1097.1	0.0	-11.1	-81.7	7.2	44	0.3 (0.2-0.7)	0.7 (0.5-1.5)

Supporting Information for

Imbalance in the modern hydrologic budget of topographic catchments along the western slope of the Andes (21–25°S)

David F. Boutt[1], Lilly G. Corenthal[1], Scott A. Hynek[2], LeeAnn Munk[3],

[1] Department of Geosciences, University of Massachusetts-Amherst, Amherst, MA, USA
[2] Earth and Environmental Systems Institute and Department of Geosciences, Pennsylvania State University, University Park, PA, USA
[3] Department of Geological Sciences, University of Alaska-Anchorage, Anchorage, AK, USA

Contents of this file

Text S1.

Calculation of Median, Lower and Upper Precipitation Bounds. To incorporate uncertainty into our analysis of precipitation in the regional precipitation dataset we consider 3 instances of precipitation estimates. The median precipitation value is the processed TRMM 2B31 dataset from [*Bookhagen and Strecker, 2008*], which has already been evaluated against gauge data in the region and is shown to be a good estimate of precipitation. To evaluate the bias of TRMM 2B31 in this region we can compare the satellite estimates against station data from Direccion General de Aguas (DGA) (Figure S1) in Figure S2. Specific station data are provided in Table 1. While the fit between the remote sensed and station data is very good, we consider two different scenarios for estimating precipitation bias. In each case ,we modify the magnitude of the spatial distribution of precipitation using the TRMM data to calculate both a lower and upper bound precipitation values. A power law is fit to the data in the region of the greatest misfit (< 75 mm/yr) in the TRMM dataset. Functions fit to the lower and upper bounds are used to calculate a modified precipitation map and for the corresponding water balance calculations. For both bounds for values greater than 75 mm/yr we simply revert back to the TRMM 2B31 data. These estimates capture more than a 100% of variation in precipitation estimates.

Text S2.

Expanded Groundwater Recharge Methods

Given abundant chlorine (Cl) in volcanic glass (~0.1 weight %) and biotite (~0.2 weight %) from ignimbrites in the region we allow (in the upper-end recharge scenario) for the potential that 50 mg/l of Cl^- in groundwater could be sourced from rock weathering.

The basis for the GW_{RCH} estimates is data derived from over 600 water samples collected between 2011 and 2014. All samples were collected in clean HDPE bottles after passing through a 0.45 µm filter. Samples were shipped to the University of Alaska Anchorage where all chemical analyses were performed. Sample dilutions based on specific conductance were performed prior to analysis of Cl^- by ion chromotagraphy. The isotopic composition of water samples (δ^2H, $\delta^{18}O$) was measured by a Picarro L-1102i WS-CRDS analyzer (Picarro, Sunnyvale, CA).

Searching our water sample database revealed 9 wells and 2 springs sampled 1 to 6 times within the SdA watershed and 6 wells sampled by *Cervetto Sepulveda* [2012] in the Chilean Puna Plateau that fit our criteria for CMB calculations (Figure 2). Table 1 lists the details of the repeated sampling of each sample site and precipitation characteristics. These sites are located in recharge zones, and yield samples with stable isotopic compositions near the global meteoric water line [*Craig*, 1961]. These criteria minimize the influences of evaporation and salt recycling known to occur in discharge zones. The Cl^- concentration was averaged for each site. Measurements of Cl^- in precipitation include 4 rain samples collected in SdA as part of this study and published measurements from the Chilean Puna Plateau [*Cervetto Sepulveda*, 2012] and Turi and Linzor region in the upper reaches of the Río Loa catchment [*Houston*, 2007, 2009].

Expanded Evapotranspiration Estimates Methods

This equation, whereby PET[mm] = 4367[m]-(0.59*ground elevation[m]), was developed by *Houston* [2006a] based on pan evaporation from 12 meteorological stations. This equation was applied to a 30 m^2 resolution Advanced Spaceborne Thermal Emission and Reflection Radiometer (ASTER) Global Digital Elevation Model (GDEM) to calculate gridded PET for the region. Polygons outlining the borders of fresh lakes and salars were manually constructed based on Landsat imagery, and estimates of PET were applied to permanent zones of discharge (salars and fresh lakes). The mean PET (mm/year) for each polygon (m^2) is used to derive an estimated PET from each high elevation salar or lake (m^3/s) (Figure S3 and Tables S2 and S3). To determine the actual evapotranspiration (AET) we compare our PET estimates to published AET estimates for SdA [*Mardones*, 1986; *Kampf and Tyler*, 2006] and Salar de Pedernales [*Johnson et al.*, 2010]. Mean annual AET is approximately 2% of PET for the lower D_{SdA} estimate (5.6 m^3/s) and the Salar de Pedernales, and 8% of the upper D_{SdA} estimate (22.7 m^3/s). Conservatively, we therefore consider that AET could vary from 0.5 to 8% of PET for salars in the region depending on depth to water table and other factors. We assume that AET is 80% of PET for Miniques and Miscanti Lakes (specific conductance between 7,780 and 10,640 µS/cm).

Text S3.

Evaluation of the impact of Chloride Concentration in Precipitation and Precipitation magnitude on Chloride Mass Balance Recharge Calculations. Inspecting equation 3 in the manuscript both total precipitation and the chloride concentration have a positive impact on the predicated amount of groundwater recharge. Additionally, setting the term Cl_{rw} (chloride from rock weathering) to zero we also can increase the groundwater recharge. Here, we consider the sources of uncertainty in the derived precipitation-recharge relationship in the chloride mass balance method using the median precipitation (described in S1) and an average chloride concentration of 8 mg/L and the upper precipitation bound and a high chloride concentration (16 mg/L) with no contribution of Cl from rock weathering. The resulting precipitation-recharge estimates calculated for our groundwater samples described in the text is depicted in Figure S5 along with a power law fit to the data. The estimated precipitation-recharge amounts, for observed chloride concentrations in both groundwater and precipitation fall along a distribution that is well fit by a single power law. Therefore, in the manuscript we use a single power-law to calculate recharge amounts from precipitation scenarios.

Text S4.

Groundwater Footprint and Water Table Ratio. The groundwater footprint [*Gleeson et al.*, 2012] of SdA, considering only non-anthropogenic discharge, is 5–21 times larger than the topographic watershed (Text S4, Figure S6, and Table S5), which ranks among the largest footprints of aquifers studied in the world. This is especially significant since the calculations of Gleeson et al. (2012) are based predominantly on anthropogenic discharge rates. The discharge to recharge ratio (Qr:R; [*Schaller and Fan*, 2009]), a metric of whether a basin is a groundwater importer or exporter, indicates the topographic watershed, with a Qr:R ratio of 4.9–19.9, is a strong importer of groundwater. Modern shallow groundwater and surface water inflow to SdA reasonably balance low estimates of evapotranspiration; however, modern GW_{RCH} within the topographic watershed alone cannot explain the magnitude of these fluxes. We modify the groundwater footprint calculation [*Gleeson et al., 2012]*, to include groundwater abstraction only from natural sources (evapotranspiration) in order to approximate the area required to support discharge rates. The groundwater footprint (GF) can be described according to *Gleeson et al.* [2012] by GF = A[ET/(GWR-R)], where A is the area of interest, ET is the groundwater abstraction rate, GWR is the recharge rate and R is baseflow. For the SdA topographic watershed, we calculate a groundwater footprint of 87,850-365,121 km^2, or 5-21 times the area of the topographic watershed. The range is based using median GWR and the upper and lower ranges of reasonable ET estimates.

We calculate the water table ratio (WTR) for the topographic watershed of SdA following methods outlined in *Haitjema and Mitchell Bruker* [2005] and *Gleeson et al.* [2011]. The WTR is a dimensionless criterion that describes whether the water table is likely (1) topographically controlled where the water table follows topography, or (2) recharge controlled where the water table is disconnected from topography and there is strong potential for inter-basin flow. The WTR is defined by $\log(WTR) = \log\left(\frac{RL^2}{mKHd}\right)$, with abbreviations explained in *Gleeson et al.,* [2011], where a more positive log(WTR) suggests topography controlled water tables and a more negative log(WTR) suggests recharge controlled water tables. We estimate a range of log(WTR) for the watershed from -3.6 to -5.3, which suggests s strongly recharge-controlled water table similar to those of the arid southwestern United States [*Gleeson et al., 2012*].

Text S5.

Dynamic Response Time Calculations. The residence time of a system is equated to its response time using a simple box model of an aquifer system to calculate the e-folding time, or the time to readjust to new boundary conditions. The above residence time estimate does not take into account the dynamics of the hydraulic response of the system (i.e. how changes in hydraulic head are propagated from the plateau to the basin). The dynamic response time (τ_{DRes}) of a 1-dimensional homogenous aquifer can be approximated as $\tau_{DRes} = \frac{L^2}{D} = \frac{L^2 S}{bK}$, where L is a characteristic length of the flow system (here taken as the maximum length of a flow path), D is the hydraulic diffusivity $D = \frac{Kb}{S}$, K is the hydraulic conductivity, b is the aquifer thickness (here assumed to be 500 m) and S is the aquifer storage coefficient.

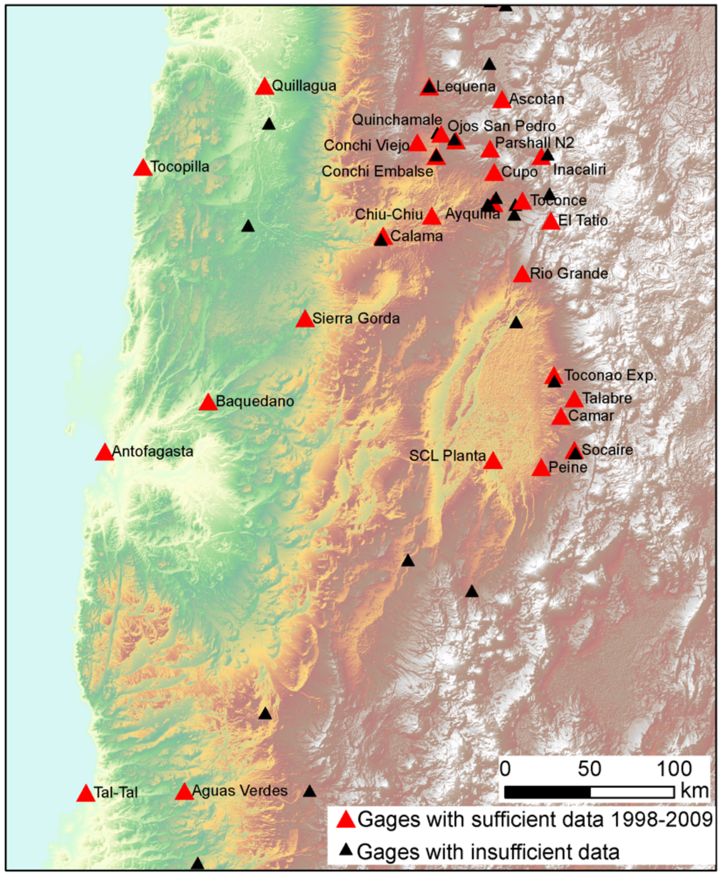

Figure S1. Meteorological stations in the Region of Antofagasta, Chile with sufficient data from the period of 1998-2009 (red triangles) and stations with discontinuous or discontinued measurements (black triangles). All stations are maintained by the Chilean Government's Direccion General de Aguas (DGA), with the exception of SCL Planta that has been maintained by the Sociedad Chilena de Litio/Rockwood Lithium, Inc/Albermarle.

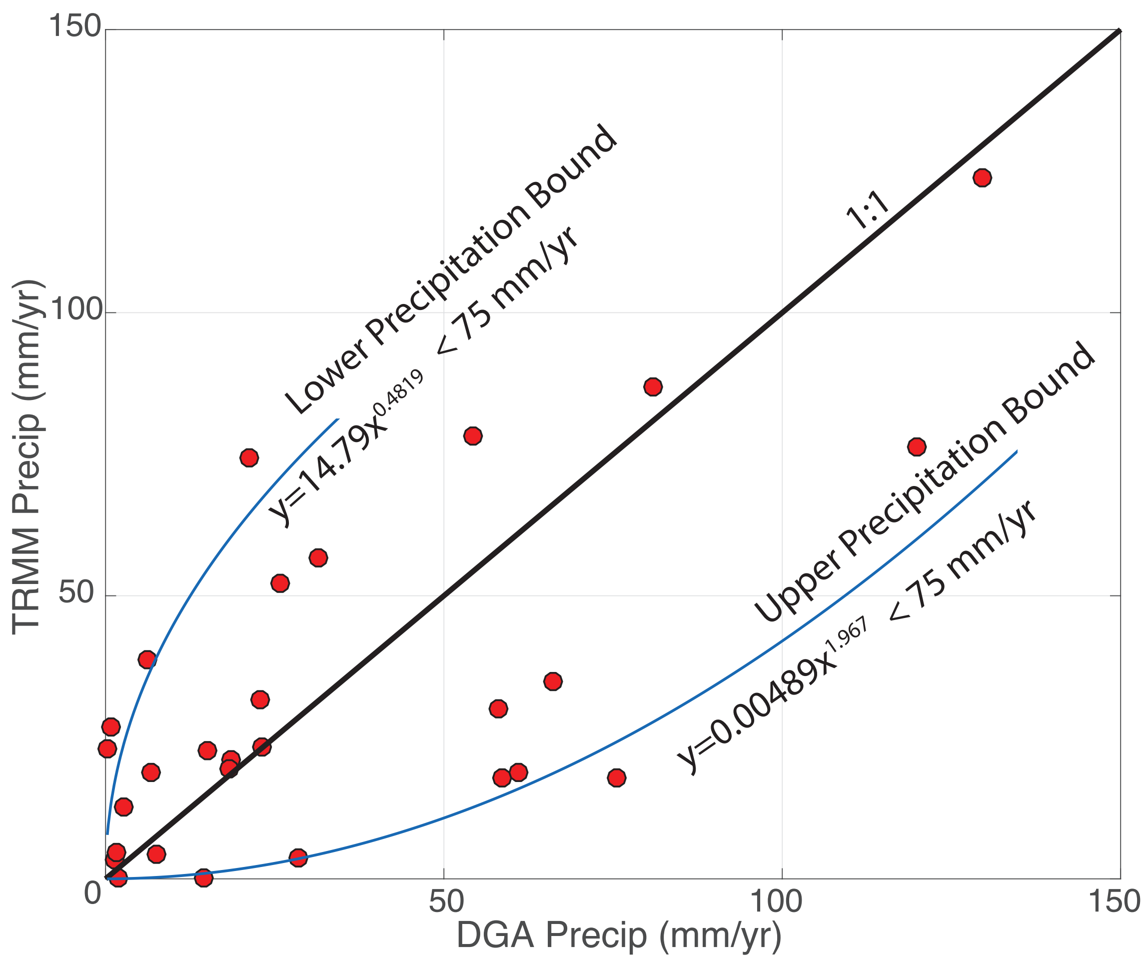

Figure S2. Comparison of gage data with remotely sensed precipitation estimates. Average annual precipitation from 1998-2009 calculated from monthly DGA raw measurements (http://snia.dga.cl/BNAConsultas/reportes) and one measurement from the Sociedad Chilena de Litio/Rockwood Lithium Inc. meteorological station. TRMM 2B31 estimate of precipitation from the TRMM 2B31 dataset [*Bookhagen and Strecker, 2008*] for sites in the Region of Antofagasta, Chile. Power functions are fit to calculate lower and upper bound precipitation maps for water balance calculations.

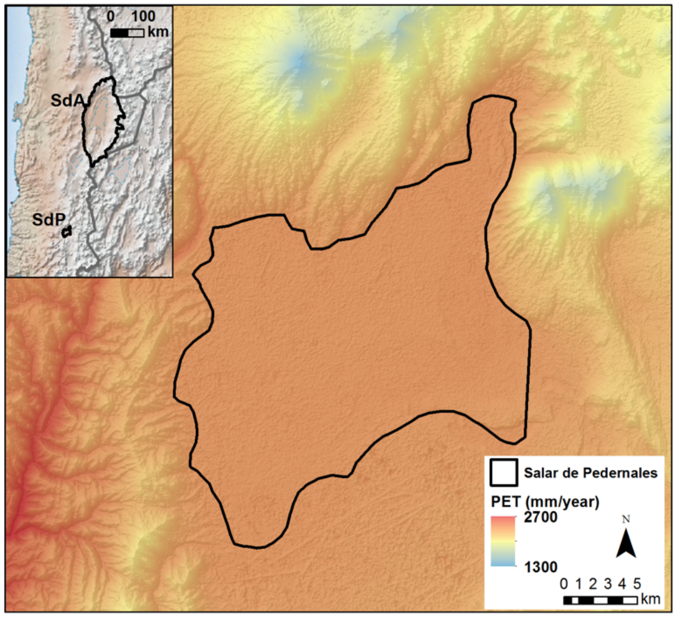

Figure S3. Map of PET computed by equation (a) in the Salar de Pedernales (SdP) region. Background is an ASTER DEM. SdP border modified from *Johnson et al.* [2010]. The SdP has a surface area of 315 km^2, average elevation of 3356 m asl and average PET of 2384 mm/year (standard deviation of 6 mm/year).

Figure S4. Conservative groundwater footprint of the SdA topographic watershed. The red zone is the topographic watershed area, and the gray shaded region is its inferred groundwater footprint based on a groundwater discharge rate of 5.6 m^3/s.

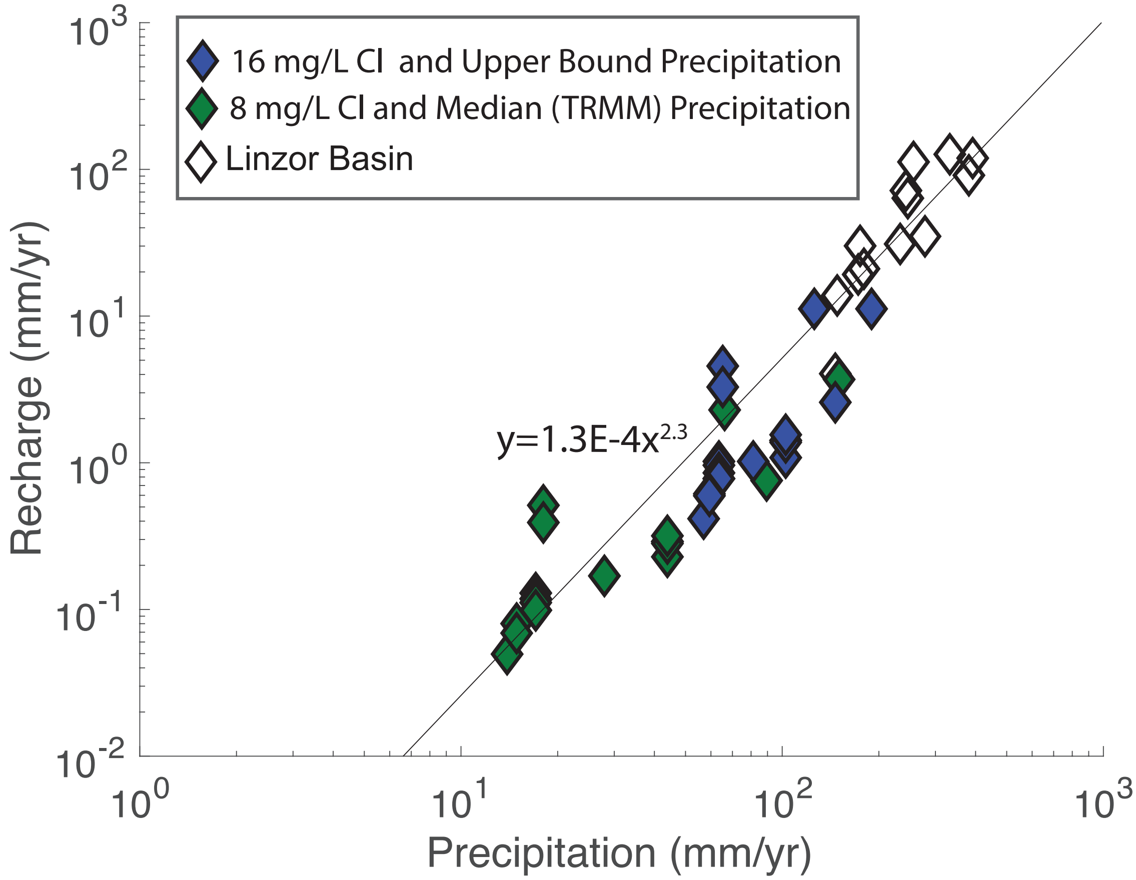

Figure S5. Precipitation-Recharge Relationship from Chloride Mass Balance Calculations.

Meteorological Station	Easting	Northing	Elevation	Distance from SdA	Precipitation Gage	Precipitation TRMM 2B31
	WGS84		m asl	km	mm/year	mm/year
Aguas Verdes	403389	7190650	1600	270	6.7	18.7
Antofagasta	358725	7389982	50	220	2	0.2
Ascotan	575136	7597754	3956	200	66.2	34.9
Ayquina	570227	7536538	3031	140	31.4	56.6
Baquedano	414749	7419946	1032	160	1.5	4.6
Calama	509841	7517409	2260	130	2.8	12.7
Camar	606276	7411224	3020	30	25.9	52.3
Chiu-Chiu	536440	7529250	2524	140	6.3	38.7
Conchi Embalse	539003	7564490	3010	170	14.5	0.1
Conchi Viejo	528514	7572609	3491	180	28.6	3.7
Cupo	570641	7554915	3600	160	81	86.8
El Tatio	601729	7526160	4320	130	129.7	123.7
Inacaliri	596588	7564208	4100	170	119.8	76.4
Lequena	535139	7605268	3320	210	61	18.7
Ojos San Pedro	568440	7568716	3800	170	58	30.0
Parshall N2	549805	7573477	3318	180	23.1	23.1
Peine	595346	7381030	2480	20	18.6	20.9
Quillagua	444822	7605629	802	250	0.4	23.0
Quinchamale	541684	7577572	3020	180	18.3	19.6
Rio Grande	585833	7495117	3250	100	58.7	17.9
SCL Plant	569278	7385349	2300	0	15.1	22.7
Sierra Gorda	467247	7468888	1616	130	0.9	26.8
Socaire	613485	7391129	3251	40	22.8	31.7
Talabre	613735	7421435	3600	40	54.4	78.1
Tal-Tal	350886	7189130	9	310	7.5	4.4
Toconao Exp.	602581	7435191	2430	40	21.3	74.3
Toconce	586111	7537991	3350	140	75.6	17.9
Tocopilla	378070	7557678	45	250	1.3	3.4

Table S1. Comparison of average annual precipitation between gage and remotely sensed sources from 1998-2009 from DGA gage measurements (http://snia.dga.cl/BNAConsultas/reportes) and one measurement from the Sociedad Chilena de Litio meteorological station (SCL Planta) with gridded precipitation from the TRMM 2B31 dataset [*Bookhagen and Strecker, 2008]* for the Region of Antofagasta, Chile.

Salar	Surface Area	Average Elevation	AET	Mean PET	Standard Deviation	Mean PET	AET/PET	Reference for AET estimate
	km^2	m asl	m^3/s	mm/year	mm/year	m^3/s	%	
Salar de Atacama	2750	2313	5.6	2999	13	262	2	Mardones, 1986 / DGA, 2010
	2864	2313	22.7	2999	13	272	8	Kampf and Tyler, 2006
Salar de Pedernales	315	3356	0.58	2384	6	24	2	Johnson et al., 2010

Table S2. Actual evapotranspiration as a fraction of potential evapotranspiration derivation for the Salar de Pedernales and Salar de Atacama.

Zone	Area (km^2)	Mean PET (m^3/s)	Mean AET (m^3/s) 2%	0.5%	8%
B	1.3*	8.2E-02	6.5E-02	6.5E-02	6.5E-02
	12.8*	7.8E-01	6.2E-01	6.2E-01	6.2E-01
	1.8	1.0E-01	2.0E-03	5.1E-04	8.2E-03
C	112.6	6.7E+00	1.3E-01	3.4E-02	5.4E-01
	13.3	7.2E-01	1.4E-02	3.6E-03	5.8E-02
	14.9	8.6E-01	1.7E-02	4.3E-03	6.9E-02
D	11.8	7.7E-01	1.5E-02	3.8E-03	6.1E-02
	22.2	1.4E+00	2.9E-02	7.2E-03	1.2E-01
	13.5	8.8E-01	1.8E-02	4.4E-03	7.0E-02
	29.6	2.1E+00	4.2E-02	1.1E-02	1.7E-01
E	3.0	2.2E-01	4.3E-03	1.1E-03	1.7E-02
	1.9	1.1E-01	2.3E-03	5.7E-04	9.1E-03
F	2.6	1.6E-01	3.3E-03	8.2E-04	1.3E-02
	11.9	8.7E-01	1.7E-02	4.4E-03	7.0E-02
	15.5	9.2E-01	1.8E-02	4.6E-03	7.3E-02
G	8.3	4.9E-01	9.9E-03	2.5E-03	3.9E-02
	71.4	4.3E+00	8.6E-02	2.1E-02	3.4E-01
	39.2	2.3E+00	4.5E-02	1.1E-02	1.8E-01
	0.6	3.2E-02	6.4E-04	1.6E-04	2.6E-03
	1.3	6.4E-02	1.3E-03	3.2E-04	5.2E-03
	1.2	6.2E-02	1.2E-03	3.1E-04	5.0E-03
	105.0	5.9E+00	1.2E-01	3.0E-02	4.7E-01
H	58.1	4.8E+00	9.6E-02	2.4E-02	3.8E-01
	51.8	3.0E+00	6.0E-02	1.5E-02	2.4E-01
I	0.9	5.0E-02	1.0E-03	2.5E-04	4.0E-03
	2.8	1.5E-01	3.0E-03	7.6E-04	1.2E-02
	0.6	3.2E-02	6.4E-04	1.6E-04	2.5E-03
	1.8	9.4E-02	1.9E-03	4.7E-04	7.5E-03
	16.9	9.1E-01	1.8E-02	4.5E-03	7.3E-02
	1.9	1.0E-01	2.0E-03	5.0E-04	8.0E-03
	0.2	1.1E-02	2.2E-04	5.5E-05	8.8E-04
	5.2	3.0E-01	6.0E-03	1.5E-03	2.4E-02
	15.3	9.5E-01	1.9E-02	4.8E-03	7.6E-02
	7.3	3.7E-01	7.5E-03	1.9E-03	3.0E-02
	358.8	2.5E+01	4.9E-01	1.2E-01	2.0E+00
J	120.5	8.2E+00	1.6E-01	4.1E-02	6.6E-01
	0.4	2.2E-02	4.3E-04	1.1E-04	1.7E-03
	2.2	1.1E-01	2.2E-03	5.6E-04	9.0E-03
	0.9	4.7E-02	9.3E-04	2.3E-04	3.7E-03
	0.8	4.0E-02	7.9E-04	2.0E-04	3.2E-03
	12.5	6.9E-01	1.4E-02	3.5E-03	5.5E-02
J	3.3	1.8E-01	3.6E-03	9.0E-04	1.4E-02
	1.2	6.4E-02	1.3E-03	3.2E-04	5.1E-03
	34.1	1.9E+00	3.7E-02	9.3E-03	1.5E-01
	22.9	1.2E+00	2.5E-02	6.1E-03	9.8E-02
	4.9	2.6E-01	5.3E-03	1.3E-03	2.1E-02
	6.9	3.8E-01	7.6E-03	1.9E-03	3.0E-02
	1.8	1.0E-01	2.0E-03	5.0E-04	8.0E-03
	33.5	1.9E+00	3.7E-02	9.3E-03	1.5E-01
K	81.0	5.3E+00	1.1E-01	2.6E-02	4.2E-01
	19.1	1.3E+00	2.5E-02	6.3E-03	1.0E-01
	141.5	9.3E+00	1.9E-01	4.6E-02	7.4E-01
	2.1	1.1E-01	2.3E-03	5.7E-04	9.1E-03
	1.9	1.0E-01	2.0E-03	5.1E-04	8.1E-03
	2.1	1.1E-01	2.3E-03	5.7E-04	9.2E-03
L	113.2	8.3E+00	1.7E-01	4.2E-02	6.7E-01
	1091.5	8.0E+01	1.6E+00	4.0E-01	6.4E+00
	154.0	1.1E+01	2.2E-01	5.4E-02	8.6E-01
	12.1	7.6E-01	1.5E-02	3.8E-03	6.1E-02
	20.8	1.4E+00	2.9E-02	7.2E-03	1.1E-01
M	119.4	8.3E+00	1.7E-01	4.2E-02	6.7E-01
	5.4	2.9E-01	5.7E-03	1.4E-03	2.3E-02
	12.8	6.9E-01	1.4E-02	3.4E-03	5.5E-02
	115.7	6.4E+00	1.3E-01	3.2E-02	5.1E-01
	1.0	5.2E-02	1.0E-03	2.6E-04	4.2E-03
	2.9	1.6E-01	3.2E-03	8.0E-04	1.3E-02
	0.8	4.7E-02	9.4E-04	2.3E-04	3.8E-03
	1.5	8.2E-02	1.6E-03	4.1E-04	6.5E-03
	3.7	2.1E-01	4.2E-03	1.0E-03	1.7E-02
	5.4	3.0E-01	6.1E-03	1.5E-03	2.4E-02
N	247.5	2.1E+01	4.1E-01	1.0E-01	1.6E+00
	19.9	1.4E+00	2.8E-02	7.0E-03	1.1E-01
	7.3	4.3E-01	8.6E-03	2.2E-03	3.4E-02
	0.5	3.1E-02	6.1E-04	1.5E-04	2.5E-03
	98.6	7.1E+00	1.4E-01	3.6E-02	5.7E-01
	24.4	1.6E+00	3.2E-02	7.9E-03	1.3E-01
O	144.9	9.8E+00	2.0E-01	4.9E-02	7.9E-01
	0.6	3.4E-02	6.8E-04	1.7E-04	2.7E-03
	0.8	4.1E-02	8.2E-04	2.1E-04	3.3E-03
	2.5	1.4E-01	2.7E-03	6.8E-04	1.1E-02
	0.6	3.3E-02	6.6E-04	1.7E-04	2.7E-03

Table S3. Summary of land type, surface area, mean annual potential evapotranspiration (PET) and actual evapotranspiration (AET) for the discharge zone polygons in all considered watersheds. Each lettered watershed includes all cumulative discharge zones in the smaller watersheds. Starred areas in watershed B are Miscanti and Miniques lakes where AET is assumed to be 80 % of PET.

Variable	Abbreviation	Value
Surface area (km^2)	A	17,257
Discharge (m^3/s)	ET	5.6 to 22.7
Recharge (m^3/s)	GWR	1.1
Baseflow contribution (m^3/s)	R	0
Groundwater Footprint (km^2)	GF	87,850 to 356,120
Groundwater stress indicator	GF/A	5 to 21

Table S4. Groundwater footprint calculations for the SdA topographic watershed. Values are specific to SdA and variables and calculations described in *Gleeson et al.* [2012]. Discharge estimates from Mardones [1986] and *Kampf and Tyler* [2006]. We consider an R of 0 consistent with the more conservative water budget conceptualization.

Description	Abbreviation	Value
Areal recharge rate (mm/year)	R	2.5
Distance between surface water bodies (km)	L	10
Hydraulic conductivity (m/day)	K	1 to 10
Average vertical extent of groundwater flow system (m)	H	100 to 500
Maximum terrain rise (m)	d	3700
Constant (unitless)	m	8
log Water Table Ratio	log(WTR)	-3.6 to -5.3

Table S5. Water Table Ratio for the SdA topographic watershed. The average areal recharge rate is calculated based on the raster of GWR presented in Figure 3b, and the maximum terrain rise is derived from an ASTER DEM. Values approximate bulk aquifer properties for the SdA. We copy the values presented in *Gleeson et al.* [2011] for distance between surface water bodies, and more conservative estimate for the average vertical extent of the flow system.

Observation Point ID	Hydraulic Head Constraints (m asl)		Simulated initial heads (m asl)		Total change in head over simulation (m)		Reference for Hydraulic Head Constraints	Notes
	Modern	*Paleo*	Restrictive Case	Conducive Case	Restrictive	Conducive		
1	2309	2314	2311	2315	<1	<1	Field Measured Water Levels	Paleo Head of +5 m is estimated based on position relative to Tulan Wetlands
2	2310	2315	2311	2315	5	5	Field Measured Water Levels	Paleo Head of +5 m is estimated based on position relative to Tulan Wetlands
3	2498	2509	2335	2328	20	10	Betancourt et al., 2000 - Tulan Wetlands	Rio Tulan deposits showed a rise of ~11 m above currrent levels between 8.2 and 3.0 ky BP, Observed heads based on approximate location of modern spring disharge
4	2692	2702	2602	2345	25	15	Betancourt et al., 2000 - Taranje Wetlands	Tarajne paleowetland deposits are at a higher elevation than the Tulan deposits. Taranje deposits date between 15.4 and 9.0 ky BP, Observed heads based on approximate location of modern spring disharge
5	2960	2975	2964	2390	180	25	Springs at Imilac and Punta Negra Quade et al 2008 - Midpoint ground elevation between the Salar de Imilac (2970 m asl) & Salar de Punta Negra (2950 m asl)	SdI & SdP are south of SdA, so approximate elevations are projected onto a similar elevation on east side (where the model geometry was derived), note that Imilac springs are fault controlled according to Quade, Observed heads based on approximate location of modern spring disharge
6	4210	4240	3980	3842	460	350	Cervetto (2012) Wells - LA and LAAR wells , Grosjean et al., 1995	Water Elevations in LA and LAAR series wells from Anexo G of Cervetto's thesis range from 4208-4216m, Laguna Tuyajito esimtates of +20-40 m
7	4320	4345	4005	3916	460	350	Cervetto (2012) Wells - PN and PNAR wells , Grosjean et al., 1995	Water Elevations in PN series wells from Anexo G of Cervetto's thesis range from 4320-4322m, Aguas Calientes IV +25 m
8	3900	4000	3993	4008	100	100	Modern Levels - Salar de Olaroz Ground elevation is 3900m (https://www.orocobre.com/PDF/NI%2043-101_Technical%20Report-Oloroz%20Project.pdf)	Paleo high stands of ~ 100 m (Grosjean et al., 1995; Placzek et al., 2006, 2013)

Table S6. Simulation results and estimates of modern and paleo hydraulic heads for specific places within the model domain. Sources of estimates and notes discussing them in 2 right-hand columns of table.